Thesis name

2022

Contents

Introduction

asd

Chapter 1

Introduction to relevant topics

1.1 Graphene

Graphene is a two-dimensional lattice of carbon atoms, arranged in a honeycomb structure as shown in the figure 1.1 Although it is straightforward to build many layers of these lattices (a substance known as graphite), it was long thought that a purely two-dimensional lattice would be unstable to thermal fluctuations and impossible to create. This changed in 2004 when Andre Geim and Konstantin Novoselov succeeded in isolating two-dimensional graphene [1]. For this, they won the 2010 Nobel prize. As we now show, the band structure of graphene is particularly interesting.

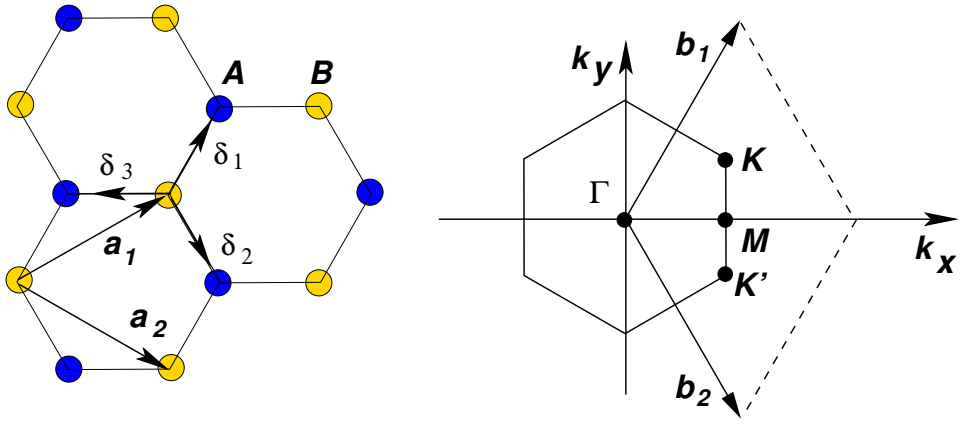

Figure 1.1: On the left there is the lattice structure of graphene made out of two interpenetrating triangular lattices (a_1 and a_2 are the lattice unit vectors, and δ_i with $i \in 1, 2, 3$ are the nearest neighbors. On the right the corresponding Brillouin zone, the Dirac cones are located at the K_0 and K_1 points) [2]

We define the primitive lattice vectors $\mathbf{a}_1$ and $\mathbf{a}_2$ as follows:

$$\mathbf{a}_1 = \frac{a}{2}\begin{bmatrix} 3 \\ \sqrt{3} \end{bmatrix} \qquad \mathbf{a}_2 = \frac{a}{2}\begin{bmatrix} 3 \\ -\sqrt{3} \end{bmatrix} \tag{1.1}$$

Where a is the distance between two neighboring atoms, which in graphene is $\approx 1.4 \times 10^{-10}$m. The sublattice A is defined as all the points $\mathbf{r} = n_1\mathbf{a}_1 + n_2\mathbf{a}_2$ with $n_i \in \mathbb{Z}$ (yellow points in figure 1.1), sublattice B is defined as all points $\mathbf{r} = n_1\mathbf{a}_1 + n_2\mathbf{a}_2 + \boldsymbol{\delta}$ with $\boldsymbol{\delta} = (a, 0)$ (blue points in figure 1.1).

The reciprocal lattice vectors $\mathbf{b}_i$ are the vectors that satisfy $\mathbf{a}_i \cdot \mathbf{b}_j = \delta_{ij}$ and are equal to

$$\mathbf{b}_1 = \frac{2\pi}{3a}\begin{bmatrix} 1 \\ \sqrt{3} \end{bmatrix} \qquad \mathbf{b}_2 = \frac{2\pi}{3a}\begin{bmatrix} 1 \\ -\sqrt{3} \end{bmatrix} \tag{1.2}$$

This reciprocal lattice is also triangular. The Brillouin zone is constructed in the usual manner by drawing perpendicular boundaries between the origin and each other point in the reciprocal lattice giving rise to a hexagonal Brillouin zone with $\mathbf{K}_0$ and $\mathbf{K}_1$ as the vertices of the hexagon, where

$$\mathbf{K}_0 = \frac{1}{3}(2\mathbf{b}_1 + \mathbf{b}_2) \qquad \mathbf{K}_1 = \frac{1}{3}(\mathbf{b}_1 + 2\mathbf{b}_2)$$

$$\mathbf{K}_0 = \frac{2\pi}{3a}\left(1, \frac{1}{\sqrt{3}}\right) \qquad \mathbf{K}_1 = \frac{2\pi}{3a}\left(1, -\frac{1}{\sqrt{3}}\right) \tag{1.3}$$

The tight binding approach

To investigate the band structure of graphene, we are going to use the tight binding approach [3, 4]. First we write the Hamiltonian.

$$H = \frac{\mathbf{p}^2}{2m} + \sum_{\mathbf{R}\in C} V_a(x - \mathbf{R}) \tag{1.4}$$

Where V_a is the potential of the single carbon atom, the set
$C = \{n_1\mathbf{a}_1 + n_2\mathbf{a}_2 + \nu\boldsymbol{\delta} \,|\, n_1, n_2 \in \mathbb{Z},\, \nu \in \{0, 1\}\}$ is the set of all the positions of the atoms.
We can re-write the potential of the Hamiltonian in this more convenient manner.

$$\sum_{\mathbf{R}\in C} V_a(x - \mathbf{R}) = V_a(x) + V'(x) \tag{1.5}$$

Where $V'(x)$ the potential of the other atoms, this way the can be divided in two parts:

$$H = \underbrace{\frac{\mathbf{p}^2}{2m} + V_a(x)}_{\substack{\text{single-atom} \\ \text{Hamiltonian}}} + \underbrace{V'(x)}_{\text{perturbation}} \tag{1.6}$$

Let $|n, \mathbf{R}\rangle$ be the n-th eingenstate of the Hamiltonian of single carbon atom placed in $\mathbf{R}$. Due to translational symmetry, the wave function must satisfy the Bloch theorem, this tells us that the eingenstates of the Hamiltonian can be written as

$$|n, \nu, \mathbf{k}\rangle = \sum_{\mathbf{R}_\nu \in C_\nu} e^{i\mathbf{k}\cdot\mathbf{R}_\nu} |n, \mathbf{R}_\nu\rangle \tag{1.7}$$

with $\nu \in \{0, 1\}$ and C_ν si defined as

$$C_\nu = \{n_1\mathbf{a}_1 + n_2\mathbf{a}_2 + \nu\boldsymbol{\delta} \,|\, n_1, n_2 \in \mathbb{Z}\}$$

With this we can now calculate the matrix elements of the Hamiltonian

$$\big\langle n, \nu, \mathbf{k}\big|H\big|n', \nu', \mathbf{k}'\big\rangle = \sum_{\mathbf{k}\mathbf{k}', \mathbf{R}\mathbf{R}'} e^{i\mathbf{k}\cdot(\mathbf{R}+\nu\boldsymbol{\delta}) - i\mathbf{k}'\cdot(\mathbf{R}+\nu'\boldsymbol{\delta})} \big\langle n, \nu, \mathbf{R}\big|H\,\big|n', \nu', \mathbf{R}'\big\rangle \tag{1.8}$$

Since the matrix elements inside the summation don't depend on k we have that the terms with $k \neq k'$ are equal to zero. So the equation above becomes

$$\big\langle n, \nu, \mathbf{k}\big|H\big|n', \nu', \mathbf{k}'\big\rangle = \big\langle n, \nu, \mathbf{k}\big|H\big|n', \nu', \mathbf{k}\big\rangle \delta_{\mathbf{k},\mathbf{k}'}$$

This means that

$$\big\langle n, \nu, \mathbf{k}\big|H\big|n', \nu', \mathbf{k}\big\rangle = \sum_{\mathbf{k}, \mathbf{R}\mathbf{R}'} e^{i\mathbf{k}\cdot(\mathbf{R}-\mathbf{R}'+\nu\boldsymbol{\delta}-\nu'\boldsymbol{\delta})} \big\langle n, \nu, \mathbf{R}\big|H\,\big|n', \nu', \mathbf{R}'\big\rangle$$

And, since it only depends on $\mathbf{R} - \mathbf{R}'$ we have that

$$\big\langle n, \nu, \mathbf{k}\big|H\big|n', \nu', \mathbf{k}\big\rangle = \sum_{\mathbf{k}, \mathbf{R}} e^{i\mathbf{k}\cdot\mathbf{R} + i(\nu-\nu')\mathbf{k}\cdot\boldsymbol{\delta}} \big\langle n, \nu, \mathbf{R}\big|H\,\big|n', \nu', \mathbf{0}\big\rangle \tag{1.9}$$

Now we need to calculate the matrix elements $\big\langle n, \nu, \mathbf{R}\big|H\,|n', \nu', \mathbf{0}\rangle$. Using equation 1.6 we get that if $\mathbf{R} = \mathbf{0}$

$$\big\langle n, \nu, \mathbf{0}\big|H\,\big|n', \nu', \mathbf{0}\big\rangle = E_n \big\langle n, \nu, \mathbf{0}\,\big|n', \nu', \mathbf{0}\big\rangle + \big\langle n, \nu, \mathbf{0}\big|V'(\mathbf{r})\,\big|n', \nu', \mathbf{0}\big\rangle \tag{1.10}$$

For $\nu = \nu'$ the first term ($E_n \big\langle n, \nu, \mathbf{0}\,|n', \nu, \mathbf{0}\big\rangle = \delta_{nn'}$) and the second term, which is called crystal field integral is usually neglected because in most cases they simply produce a rigid shift of the energy bands $E_n(\mathbf{k})$ without affecting their dispersion. [5]
For $\nu \neq \nu'$ the second term is much bigger than the first one, so

$$\big\langle n, \nu, \mathbf{0}\big|H\,\big|n', \nu', \mathbf{0}\big\rangle \approx E_n \delta_{nn'}\delta_{\nu\nu'} + \big\langle n, \nu, \mathbf{0}\big|V'(\mathbf{r})\,\big|n', \nu', \mathbf{0}\big\rangle\,(1 - \delta_{\nu\nu'}) \tag{1.11}$$

Since we consider the wavefunctions as strongly localized, the second term is much smaller than the first one, so we can ignore it.
Usually the matrix elements $\big\langle n, \nu, \mathbf{0}\big|V'(\mathbf{r})\,|n', \nu', \mathbf{0}\big\rangle$ are conveniently expressed

$\langle\ s\ ,\nu,\mathbf{0}\big\vert V'(\mathbf{r})\ \vert\ s\ ,\nu',\mathbf{0}\rangle = V(ss\sigma)$
$\langle\ s\ ,\nu,\mathbf{0}\big\vert V'(\mathbf{r})\ \vert p_x,\nu',\mathbf{0}\rangle = l_x V(sp\sigma)$
$\langle p_x,\nu,\mathbf{0}\big\vert V'(\mathbf{r})\ \vert p_x,\nu',\mathbf{0}\rangle = l_x^2 V(pp\sigma) + (1-l_x^2)V(pp\pi)$
$\langle p_x,\nu,\mathbf{0}\big\vert V'(\mathbf{r})\ \vert p_y,\nu',\mathbf{0}\rangle = l_x l_y\left[V(pp\sigma) - V(pp\pi)\right]$
$\langle p_x,\nu,\mathbf{0}\big\vert V'(\mathbf{r})\ \vert p_z,\nu',\mathbf{0}\rangle = l_x l_z\left[V(pp\sigma) - V(pp\pi)\right]$

Table 1.1: Here we have defined $\boldsymbol{\delta} = (l_x, l_y, l_z)|\delta|$

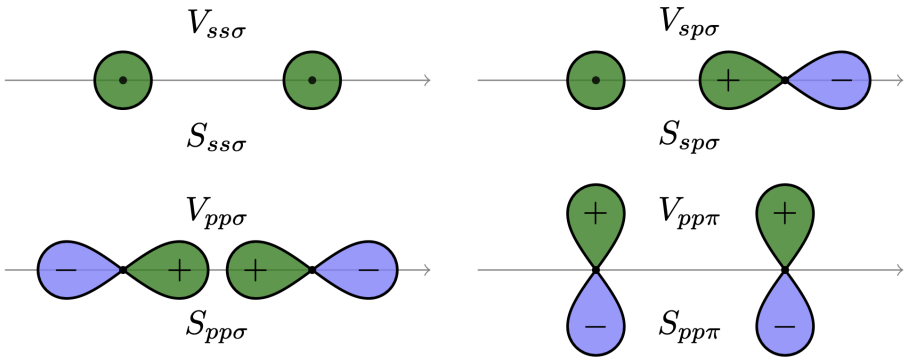

Figure 1.2: Each one of the potentials $V(ss\sigma), V(sp\sigma), V(pp\sigma), V(pp\pi)$ represent a different kind of bonding between the two orbitals. The first two indices represent the orbitals (s and p), the last one represent the bonding type (σ and π)

in terms of a a small number of independent parameters, and are evaluated either analytically, or numerically, or semi-empirically.

In the case of carbon atoms we only need to work with atomic orbitals of type s and p, this means that the independent matrix elements to evaluate are shown in table 1.1

These parameters can be pictorially shown in figure 1.2
The Hamiltonian matrix should be a 8×8 matrix. Nevertheless, from group theory we know that at a general point k the Bloch functions derived from s, p_x and p_y atomic functions never mix with the Bloch function p_z because of the symmetry operation of reflection through the xy plane. We can thus classify the energy states as even or odd with respect to this transformation; the former give rise to the so-called σ-bands and the latter to the so-called π-bands. Moreover, the problem is decomposed into two decoupled subproblems and, instead of diagonalizing a single 8×8 matrix, we have to cope separately with a 2×2 matrix (π-bands) and a 6×6 matrix (σ-bands).

Fortunately the σ-bands are fully below the Fermi-level, so they don't have any contribution to the electron-transport phenomenon, so we only have to deal with the 2×2 matrix of the π-bands

$$\langle p_z, \nu, \mathbf{0} | H | p_z, \nu', \mathbf{0} \rangle = \begin{bmatrix} E_p & V(pp\pi) \\ V(pp\pi) & E_p \end{bmatrix} \tag{1.12}$$

Now we can evaluate equation 1.9 considering just the nearest-neighbors

$$\langle p_z, 0, \mathbf{k} | H | p_z, 0, \mathbf{k} \rangle = \sum_{\mathbf{k},\mathbf{R}} e^{i\mathbf{k}\cdot\mathbf{R}} \langle p_z, 0, \mathbf{R} | H | p_z, 0, \mathbf{0} \rangle \approx E_p \tag{1.13}$$

$$\begin{aligned} \langle p_z, 0, \mathbf{k} | H | p_z, 1, \mathbf{k} \rangle =& \sum_{\mathbf{k},\mathbf{R}} e^{i\mathbf{k}\cdot\mathbf{R} + i\mathbf{k}\cdot\boldsymbol{\delta}} \langle p_z, 0, \mathbf{R} | H | p_z, 1, \mathbf{0} \rangle \approx \\ \approx& \sum_i e^{i\mathbf{k}\cdot\delta_i} V(pp\pi) \equiv \\ \equiv& V(pp\pi) F(\mathbf{k}) \end{aligned} \tag{1.14}$$

Where $F(\mathbf{k})$ is defined as the geometrical form factor, and it is equal to

$$F(\mathbf{k}) = \sum_{\boldsymbol{\delta}_i} e^{i\mathbf{k}\cdot\boldsymbol{\delta}_i} = 1 + 2\cos\frac{k_x\delta}{2} e^{-i\frac{\sqrt{3}}{2}k_y\delta} \tag{1.15}$$

Therefore, the k-dependent Hamiltonian for the π-bands is

$$\langle p_z, \nu, \mathbf{k} | H | p_z, \nu', \mathbf{k}' \rangle = \delta_{kk'} \begin{bmatrix} E_p & V(pp\pi)F(\mathbf{k}) \\ V(pp\pi)F(\mathbf{k}) & E_p \end{bmatrix} \tag{1.16}$$

The eigenvalues of the Hamiltonian give us the dispersion relation 1.3

$$E(\mathbf{k}) = E_p + V(pp\pi)F(\mathbf{k}) \tag{1.17}$$

Near the degenerate points $\mathbf{K}_0$ and $\mathbf{K}_1$ (eq. 1.3), the geometrical form factor can be expanded in Taylor series to first order in the wavevector measured from the $\mathbf{K}_0$ and $\mathbf{K}_1$ points. The resulting expression of the form factors are

$$F_{\mathbf{K}_0}(\mathbf{k}) = -F^*_{\mathbf{K}_1}(\mathbf{k}) = -\frac{\sqrt{3}}{2}\delta(k_x - ik_y) \tag{1.18}$$

This means that the matrix Hamiltonians near the degeneracies can be recast in the form

$$H_{\mathbf{K}_0}(\mathbf{k}) = -H^*_{\mathbf{K}_1}(\mathbf{k}) = \begin{bmatrix} 0 & v_F\hbar(k_x - ik_y) \\ v_F\hbar(k_x + ik_y) & 0 \end{bmatrix}; \quad v_f = \frac{\sqrt{3}}{2}\frac{\delta}{\hbar}V(pp\pi) \tag{1.19}$$

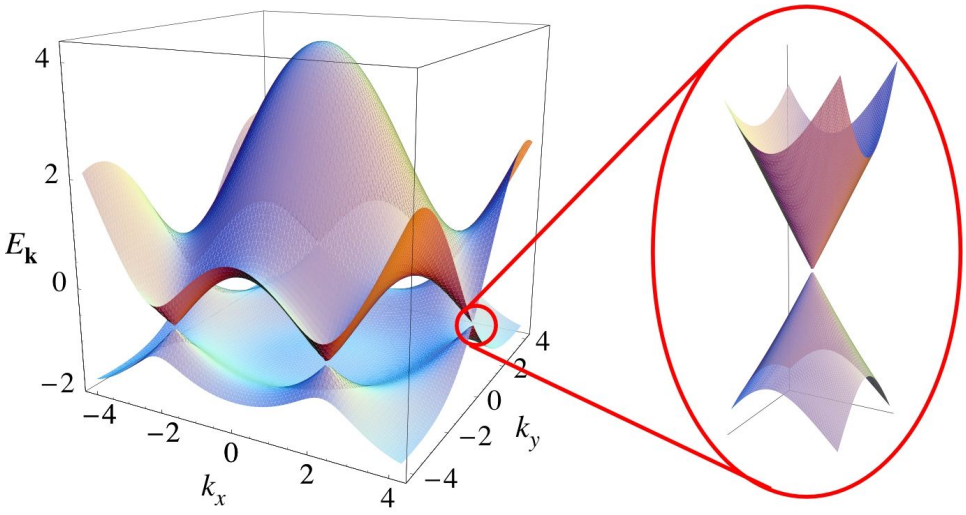

Figure 1.3: This is the dispersion relation for the single layer graphene, notice how near the vertices of the reciprocal lattice we get a cone-like dispersion relation typical of relativistic massless particles

The eigenvalues of both Hamiltonians are

$$E(k) = \pm v_F \hbar k \quad \text{with} \quad k = \sqrt{k_x^2 + k_y^2} \tag{1.20}$$

This means that electrons near the Dirac cones behave pretty much like photons, except that they move at the Fermi speed v_F instead of the speed of light

Chapter 2

Berry phase and Berry curvature

2.1 Introduction

Berry phase is the simplest demonstration of how geometry and topology can emerge from quantum mechanics and at heart of the quantum Hall effect.
Let us consider a physical system described by a Hamiltonian that depends on a set of parameters $\boldsymbol{\lambda} = (\lambda_1, \lambda_2, \dots)$. These parameters do not represent the degrees of freedom of the system like position and momentum, rather they describe things such as the mass of a particle, the strength of a potential and so on.
For each $H(\boldsymbol{\lambda})$ there exists a set of eigenstates such that

$$H(\boldsymbol{\lambda}) \left|n, \boldsymbol{\lambda}\right\rangle = E_n(\boldsymbol{\lambda}) \left|n, \boldsymbol{\lambda}\right\rangle \tag{2.1}$$

However the equation above does not completely determine the basis function $|n, \boldsymbol{\lambda}\rangle$; We can change arbitrarily the phase $\gamma_n(\boldsymbol{\lambda})$ of any eigenstate which is called *Berry phase*

$$|n, \boldsymbol{\lambda}\rangle \to \underbrace{e^{i\gamma_n(\boldsymbol{\lambda}(t))}}_{\text{Berry phase}} |n, \boldsymbol{\lambda}\rangle \tag{2.2}$$

Suppose we start off with a Hamiltonian and then we slowly change the parameters for a time T until it reaches a different Hamiltonian, this means that $\boldsymbol{\lambda} = \boldsymbol{\lambda}(T)$. For the adiabatic theorem we can say that if we start on an energy eigenstate, and the system changes slowly enough, [1] and has no

[1] How slow you have to be in changing the parameters depends on the energy gap from the state you're in to the nearest other state. The smaller the gap, the slower you have to change the parameters. A way of showing this without doing long calculations is the following:
We know from the Heisenberg uncertainty principle that $T\Delta E \geq \hbar/2$. We want the uncertainty in the Energy to be way smaller than the energy gap $E_g \gg \Delta E$, so $E_g \gg \frac{\hbar}{2T}$, therefore if we make T big enough it can be achieved

degeneracies, then the system will cling on that energy eigenstate.
This means that the equation of motion of a particle that for time $t = 0$ is equal to $|\psi_n(t=0)\rangle = |n, \boldsymbol{\lambda}(0)\rangle$ is

$$|\psi_n(t)\rangle = \underbrace{e^{i\gamma_n(\boldsymbol{\lambda}(t))}}_{\text{Berry phase}} \cdot \underbrace{e^{-\frac{i}{\hbar}\int_0^t E_n(\boldsymbol{\lambda}(t'))dt'}}_{\text{dynamical phase}} |n, \boldsymbol{\lambda}(t)\rangle \tag{2.3}$$

Where the first exponent comes from eq. 2.2. We now insert the equation above into the time-dependent Shrodinger equation

$$i\hbar\partial_t|\psi_n(t)\rangle = H(\boldsymbol{\lambda}(t))|\psi_n(t)\rangle \tag{2.4}$$

By plugging equation 2.3 into the *right* term term of equation 2.4 we get we get that

$$H(\boldsymbol{\lambda}(t))|\psi_n(t)\rangle = E_n(t)\,|\psi_n(t)\rangle \tag{2.5}$$

Andy By plugging equation 2.3 into the *left* term term of equation 2.4 we get we get that

$$i\hbar\partial_t|\psi_n(t)\rangle = -\hbar\dot{\gamma}_n(t)|\psi_n(t)\rangle + E_n(t)|\psi_n(t)\rangle + e^{i\phi_n(t)}\partial_t|n,t\rangle \tag{2.6}$$

where we have defined $e^{i\phi_n(t)} \equiv e^{i\gamma_n(\boldsymbol{\lambda}(t))}e^{-\frac{i}{\hbar}\int_0^t E_n(\boldsymbol{\lambda}(t'))dt'}$

By equating the right terms in equations 2.5 and 2.6 we get that

$$i\hbar e^{i\phi_n t(t)}\partial_t|n,t\rangle = \hbar\dot{\gamma}_n(t)\,|\psi_n(t)\rangle = \hbar\dot{\gamma}_n(t)e^{i\phi_n(t)}\,|n,t\rangle \tag{2.7}$$

now we multiply the term on the left and on the right of equation 2.7 by $\hbar^{-1}e^{-i\phi_n(t)}\,\langle n,t|$

$$\dot{\gamma}_n(t) = i\,\langle n,t|\,\partial_t\,|n,t\rangle \tag{2.8}$$

We can re-express it in terms of $\boldsymbol{\lambda}$

$$\dot{\gamma}_n(t) = \dot{\boldsymbol{\lambda}} \cdot \underbrace{i\,\langle n,t|\,\partial_{\boldsymbol{\lambda}}\,|n,t\rangle}_{\equiv \mathbf{A}_n(\boldsymbol{\lambda})} \tag{2.9}$$

Where $\mathbf{A}_n(\boldsymbol{\lambda})$ called the **Berry connection** This means that we can calculate the total change in $\gamma_n(t)$ can be obtained by doing a line integral in the space of parameters $\boldsymbol{\lambda}$ over the path $\mathcal{P}$ of values that $\boldsymbol{\lambda}$ assumes during the time evolution

$$\gamma_n = \int_{\mathcal{P}} \mathbf{A}_n(\boldsymbol{\lambda}) \cdot d\boldsymbol{\lambda} \tag{2.10}$$

$$|n, \boldsymbol{\lambda}\rangle \to e^{if_n(\boldsymbol{\lambda})}\,|n, \boldsymbol{\lambda}\rangle \tag{2.11}$$

Keep in mind however that the eigenstates are defined up to a phase, meaning that we can re-define the base vectors like so (equation 2.11). If we apply this substitution into the formula of $\mathbf{A}_n$ we have that

$$\mathbf{A}_n(\boldsymbol{\lambda}) = i \langle n,t| \partial_{\boldsymbol{\lambda}} |n,t\rangle \to i \langle n,t| \partial_{\boldsymbol{\lambda}} |n,t\rangle - \partial_{\boldsymbol{\lambda}} f_n(\boldsymbol{\lambda})$$

$$\mathbf{A}_n \to \mathbf{A}_n - \partial_{\boldsymbol{\lambda}} f_n \tag{2.12}$$

So the system is invariant under the gauge transformation in equation 2.12. If we do this transformation to equation 2.10 we have that

$$\gamma_n = \int_{\mathcal{P}} \mathbf{A}_n(\boldsymbol{\lambda}) \cdot d\boldsymbol{\lambda} - \int_{\mathcal{P}} \partial_{\boldsymbol{\lambda}} f_n(\boldsymbol{\lambda}) \cdot d\boldsymbol{\lambda} = \int_{\mathcal{P}} \mathbf{A}_n(\boldsymbol{\lambda}) \cdot d\boldsymbol{\lambda} + f(\boldsymbol{\lambda}(0)) - f(\boldsymbol{\lambda}(T))$$

This means that if the path $\mathcal{P}$ is open we can always choose a function f_n such that $f(\boldsymbol{\lambda}(0)) - f(\boldsymbol{\lambda}(T)) = \int_{\mathcal{P}} \mathbf{A}_n(\boldsymbol{\lambda}) \cdot d\boldsymbol{\lambda}$, thus we can conclude that one can always choose a suitable $f(\boldsymbol{\lambda})$ such that γ_n accumulated along the path $\mathcal{P}$ is calceled out leaving equation 2.3 with only the dynamical phase. However if the path is closed $\boldsymbol{\lambda}(0) = \boldsymbol{\lambda}(T)$, in order to make the phase change in equation 2.11 single value we must have that

$$e^{f(\boldsymbol{\lambda}(0)) - f(\boldsymbol{\lambda}(T))} = 1$$

so

$$f(\boldsymbol{\lambda}(0)) - f(\boldsymbol{\lambda}(T)) = 2n\pi \quad n \in \mathbb{R}$$

This leads us to the important result that

$$\gamma_n = \oint_{\mathcal{P}} \mathbf{A}_n(\boldsymbol{\lambda}) \cdot d\boldsymbol{\lambda} + 2n\pi \tag{2.13}$$

This time, if the line integral is not a multiple of 2π (and there is no reason why it should) there is no way of choosing a suitable f_n to cancel it out and the Berry phase in equation 2.3 is there to stay

2.2 Berry curvature

You might have noticed that equation 2.12 is analogous to what happens in Electromagnetism with the vector potential. This means that we can try using the same mathematics and see where it leads us. However, in classic and relativistic electromagnetism $\dim(\mathbf{A}_\mu)$ is equal to respectively 3 and 4, in the case of the Berry curvature it can have any integer value.

In EM from the gauge-dependent $\mathbf{A}$ are defined the gauge-indipendent field as follows:

1. in 3D the magnetic field is defined as follows $B_i = \epsilon_{ijk} \partial_j A_k$
2. in $(3+1)$D the Field tensor is defined as $F_{\mu\nu} = \partial_\mu A_\nu - \partial_\nu A_\mu$

In both cases the resulting field is asymmetric under the exchange of the indices of the derivative and the indices of the vector potential. This requirement is what makes the resulting field gauge independent.

With the same logic we can define a gauge field tensor derived from the Berry connection:

$$\boxed{\Omega^n_{\mu\nu} = \partial_\mu A^n_\nu(\boldsymbol{\lambda}) - \partial_\nu A^n_\mu(\boldsymbol{\lambda})} \tag{2.14}$$

This new field tensor is defined as **Berry curvature**, and it is gauge independent just like $\mathbf{B}$ and $F_{\mu\nu}$![2]

From now on it can be useful to introduce the external product operator $\wedge$ that act as follows: Given two vectors $\mathbf{v}$ and $\mathbf{w}$ we have that

$$\mathbf{v} \wedge \mathbf{w} \equiv v_\mu w_\nu - v_\nu w_\mu \tag{2.15}$$

With this definition we can write

$$\boldsymbol{\Omega}^n(\boldsymbol{\lambda}) = \nabla \wedge \mathbf{A}^n(\boldsymbol{\lambda}) \tag{2.16}$$

2.2.1 Other formulas for $\Omega_{\mu\nu}$

With a few mathematical steps it is possible to re cast the Berry curvature into a different form that might be useful later

$$\partial_\mu A^n_\mu = i\partial_\mu \langle n, \boldsymbol{\lambda}| \partial_\nu n, \boldsymbol{\lambda}\rangle = i \langle \partial_\mu n, \boldsymbol{\lambda}| \partial_\nu n, \boldsymbol{\lambda}\rangle + i \langle n, \boldsymbol{\lambda}| \partial_\mu \partial_\nu n, \boldsymbol{\lambda}\rangle$$

$$\boxed{\Omega^n_{\mu\nu} = i \langle \partial_\mu n| \partial_\nu n\rangle - i \langle \partial_\nu n| \partial_\mu n\rangle} \tag{2.17}$$

or, equivalently

$$\boldsymbol{\Omega}^n = i \langle \nabla n| \wedge |\nabla n\rangle \tag{2.18}$$

It is also possible to express Ω in terms of the eigenstates of the Hamiltonian with some mathematical manipulation

$$\langle n'| H |n\rangle = \delta_{n'n} \to \partial_\mu \langle n'| H |n\rangle = 0$$

$$\partial_\mu \langle n'| H |n\rangle = \langle \partial_\mu n'| H |n\rangle + \langle n'| H |\partial_\mu n\rangle + \langle n'| \partial_\mu H |n\rangle$$

$$E_n \langle \partial_\mu n'| n\rangle + E_{n'} \langle n'| \partial_\mu n\rangle = \langle n'| \partial_\mu H |n\rangle$$

$$(E_{n'} - E_n) \langle n'| \partial_\mu n\rangle = \langle n'| \partial_\mu H |n\rangle$$

$$\langle n'| \partial_\mu n\rangle = \frac{\langle n'| \partial_\mu H |n\rangle}{E_{n'} - E_n} \tag{2.19}$$

Now we write equation 2.17 like so

$$\Omega^n_{\mu\nu} = i \langle \partial_\mu n| \partial_\nu n\rangle - (\mu \leftrightarrow \nu) = i \sum_{n' \neq n} \langle \partial_\mu n| n'\rangle \langle n'| \partial_\nu n\rangle - (\mu \leftrightarrow \nu)$$

[2]The notation has changed a bit, now $A^n_\mu \equiv (\mathbf{A}_n)_\mu$

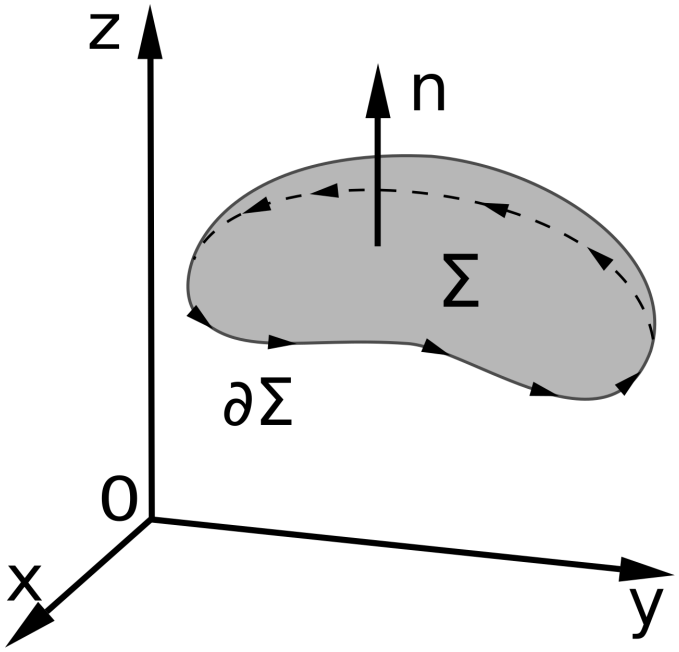

Figure 2.1: Here we divide the surface of the sphere in two different surfaces $\mathcal{A}$ and $\mathcal{B}$ that share the edge $\mathcal{P}$

By plugging in above equation 2.19 we get

$$\boxed{\Omega^n_{\mu\nu} = i \sum_{n' \neq n} \frac{\langle n | \, \partial_\mu H \, | n' \rangle \, \langle n' | \, \partial_\nu H \, | n \rangle}{(E_{n'} - E_n)^2} - (\mu \leftrightarrow \nu)} \tag{2.20}$$

This last form of the Berry curvature has the advantage that no differentiation of the wavefunction is needed. This equation also tells us that

$$\sum_n \Omega^n_{\mu\nu}(\boldsymbol{\lambda}) = 0$$

Equation 2.20 can also be written as

$$\boldsymbol{\Omega}^n = \sum_{n' \neq n} \frac{\langle n | \, \nabla H \, | n' \rangle \wedge \langle n' | \, \nabla H \, | n \rangle}{(E_{n'} - E_n)^2} \tag{2.21}$$

2.3 Stokes' Theorem

From the Stokes theorem we have that

$$\gamma_n = \oint_{\mathcal{P}} A^n_\mu \, d\lambda^\mu = \frac{1}{2} \int_\Sigma \Omega^n_{\mu\nu} \, d\lambda^\mu \wedge d\lambda^\nu \tag{2.22}$$

where we have used the Einstein convention of summation.
There is a subtelty in this last equation, as we know the Berry curvature tensor in Gauge-invariant, so the integral over the surface is too, but the integral over the closed path of the Berry connection is defined up to a factor $2n\pi$ that is gauge dependant. So is there a modulo 2π ambiguity or not?
The answer is that if γ_n is to be determined using the knowledge of $|n, \boldsymbol{\lambda}\rangle$ only on the curve $\mathcal{P}$ then it is really well defined modulo 2π. In this case we can re-write equation 2.22 as

$$\frac{1}{2}\int_{\Sigma} \Omega^n_{\mu\nu}\, d\lambda^\mu \wedge d\lambda^\nu := \oint_{\mathcal{P}} A^n_\mu\, d\lambda^\mu$$

Meaning that the integral over the surface Σ is equal to *one of the values of* the integrals along the closed path $\mathcal{P}$

But what kind of Gauge gives the "correct" answer? If we choose a gauge that is continuous and smooth everywhere along the surface Σ including on its boundary $\mathcal{P}$ then equation 2.22 becomes unambiguous.
While it is possible to make a radical gauge transformation that shifts γ_n by 2π when regarding $|n, \boldsymbol{\lambda}\rangle$ as a function defined only in the neighborhood of $\mathcal{P}$, such a gauge change cannot be smoothly continued into the interior $\mathcal{S}$ without creating a vortex-like singularity of $\gamma_n(\boldsymbol{\lambda})$.

2.4 Chern Theorem

Let's take as an example Gauss's theorem. It tells us that the flux of the field through a closed surface is equal to the charges inside.
Now let's calculate the flux of the Berry curvature through a closed surface. We can divide the closed surface as two different open surfaces that share the same edge $\mathcal{P}$.
Thanks to stokes theorem the flux through the surface $\mathcal{A}$ is $\oint_{\mathcal{P}} \mathbf{A} \cdot d\boldsymbol{\lambda}$, but the flux through the surface $\mathcal{B}$ is $-\oint_{\mathcal{P}} \mathbf{A} \cdot d\boldsymbol{\lambda}$.
Theese two integrals must be equal modulo 2π, so

$$\oint_{\mathcal{S}} \Omega^n_{\mu\nu} d\lambda^\mu \wedge d\lambda^\nu = 2\pi C \qquad C \in \mathbb{Z} \tag{2.23}$$

This means that the flux thought a closed surface of the Berry curvature is quantized

The constant C in known as the Chern number. Note that when the Chern index is nonzero, it is impossible to construct a smooth and continuous gauge over the entire surface $\mathcal{S}$. If such a gauge did exist, then we could apply Stokes' theorem directly to the entire surface and conclude that the Chern number vanishes, in contradiction with the assumption.

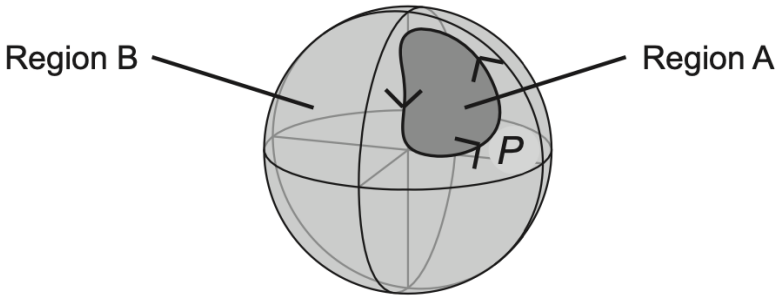

Figure 2.2: Here we divide the surface of the sphere in two different surfaces $\mathcal{A}$ and $\mathcal{B}$ that share the edge $\mathcal{P}$

But what are these "pseudo-charges" inside the closed surface that generate the flux?
In E.M. a simple way to spot charges (or monopoles) is to look at the fields and see if as some point it diverges as $1/(\mathbf{r}-\mathbf{r_0})^2$. Let's take a look at $\Omega_{\mu\nu}$ (eq. 2.20) and see if we can spot anything similar [3]

$$\Omega^n_{\mu\nu} = i \sum_{n' \neq n} \frac{\langle n| \partial_\mu H |n'\rangle \wedge \langle n'| \partial_\nu H |n\rangle}{\underbrace{[E_{n'}(\boldsymbol{\lambda}) - E_n(\boldsymbol{\lambda})]^2}_{\substack{\text{what happens if for some } \boldsymbol{\lambda}=\boldsymbol{\lambda}_d \\ \text{the two energies are the same?}}}} \tag{2.24}$$

So, suppose that for some $\boldsymbol{\lambda} = \boldsymbol{\lambda}_d$ we have that $E_n(\boldsymbol{\lambda}_d) = E_m(\boldsymbol{\lambda}_d)$, now we expand the energies near $\boldsymbol{\lambda}_d$ at first order

$$\begin{cases} E_n(\boldsymbol{\lambda}) \approx E_n(\boldsymbol{\lambda}_d) + \partial_{\boldsymbol{\lambda}} E_n|_{\boldsymbol{\lambda}=\boldsymbol{\lambda}_d} \cdot (\boldsymbol{\lambda} - \boldsymbol{\lambda}_d) \\ E_m(\boldsymbol{\lambda}) \approx E_n(\boldsymbol{\lambda}_d) + \partial_{\boldsymbol{\lambda}} E_m|_{\boldsymbol{\lambda}=\boldsymbol{\lambda}_d} \cdot (\boldsymbol{\lambda} - \boldsymbol{\lambda}_d) \end{cases}$$

This means that

$$E_n(\boldsymbol{\lambda}) - E_m(\boldsymbol{\lambda}) \approx \partial_{\boldsymbol{\lambda}}(E_n - E_m)|_{\boldsymbol{\lambda}=\boldsymbol{\lambda}_d} \cdot (\boldsymbol{\lambda} - \boldsymbol{\lambda}_d)$$

so the denominator of the berry curvature near $\boldsymbol{\lambda}_d$ goes like $1/(\boldsymbol{\lambda} - \boldsymbol{\lambda}_d)^2$.
This means that there are "charges" or "monopoles" that induce the flux through the closed surface, and they are localized where 2 (or more) energy levels cross

[3] In the equation below I expressed explicitly the $\boldsymbol{\lambda}$ dependence in the denominator and condensed the formula using the wedge product $\wedge$

Chapter 3

ValleyHall

3.1 Berry curvature in Gapped graphene

The Hamiltonian for the gapped graphene near the point K_1 and K_2 can be written as

$$H_{K_1} = H^{\dagger}_{K_2} = \begin{bmatrix} \Delta & \hbar v_F(k_x + ik_y) \\ \hbar v_f(k_x - ik_y) & \Delta \end{bmatrix} \tag{3.1}$$

Where Δ is the energy gap and v_F is the Fermi velocity. For ease of notation we are going to work with just H_{K_1} and drop the K_1,[1] and for ease of computation we define $\mathbf{q} = \hbar v_F \mathbf{k}$

$$H = \begin{bmatrix} \Delta & q_x + iq_y \\ q_x - iq_y & \Delta \end{bmatrix} = \sigma_x q_x + \sigma_y q_y + \sigma_z \Delta \equiv \boldsymbol{\sigma} \cdot \mathbf{E} \tag{3.2}$$

Here the enegry vector $\mathbf{E}$ is defined as $\mathbf{E} = (q_x, q_y, \Delta)$. The nice things about it is that $E = |\mathbf{E}| = \sqrt{q_x^2 + q_y^2 + \Delta^2}$ is the positive eigenvalue of the hamiltonian (the negative eigenvalue is just $-E$).
To calculate the Berry curvature we are first going to calculate the Berry connection 2.9, and to calultate the Berry connection we need the eigenvectors which are well known for the Hamiltonian of the form $\boldsymbol{\sigma} \cdot \mathbf{E}$.

$$|+; \theta, \phi\rangle = \begin{bmatrix} \cos\frac{\theta}{2} \\ e^{i\phi}\sin\frac{\theta}{2} \end{bmatrix} \quad |-; \theta, \phi\rangle = \begin{bmatrix} -e^{-i\phi}\sin\frac{\theta}{2} \\ \cos\frac{\theta}{2} \end{bmatrix} \tag{3.3}$$

Where θ and ϕ are the coordinates of $\mathbf{E}$ in the polar representation

Now we can calculate the Berry connection

[1] Don't worry, I'll bring it back if when we'll need it

$$A_\theta^+ = -A_\theta^- = 0 \quad A_\phi^+ = -A_\phi^- = \sin^2\frac{\theta}{2} \tag{3.4}$$

This means that the Berry curvature is

$$\Omega_{\theta\phi}^+ = -\Omega_{\theta\phi}^- = \partial_\theta A_\phi^+ = \frac{\sin\theta}{2} \tag{3.5}$$

From now on we are going to work with Ω^+ and we are going to drop the + sign to make the notation lighter.

We want to express Ω in terms of $\mathbf{q}$, however it's more convenient to write it in terms fo $\cos\theta$ and ϕ, so we do a small coordinate transformation

$$\Omega_{\theta\phi} = \frac{\partial\cos\theta}{\partial\theta}\Omega_{\cos(\theta)\phi} \to \Omega_{\cos(\theta)\phi} = \frac{1}{2} \tag{3.6}$$

Now we can easily make the transformation to express Ω in terms of $\mathbf{q}$. The Berry curvature transforms like any other tensor under coordinate transformation, so

$$\Omega_{q_xq_y} = \frac{\partial\cos\theta}{\partial q_x}\frac{\partial\phi}{\partial q_y}\Omega_{\cos(\theta)\phi} + \frac{\partial\phi}{\partial q_x}\frac{\partial\cos\theta}{\partial q_y}\Omega_{\phi\cos(\theta)} \tag{3.7}$$

That can be rewritten as

$$\Omega_{q_xq_y} = \frac{1}{2}\det\left[\frac{\partial(cos\theta,\phi)}{\partial(q_x,q_y)}\right] = \frac{1}{2}\frac{\Delta^2}{q^2E^3}(q_x+q_y-2q) \tag{3.8}$$

And finally we can express it in terms of $\mathbf{k}$

$$\Omega_{k_xk_y} = (\hbar v_F)^2\Omega_{q_xq_y} = \frac{\hbar v_F}{2}\frac{\Delta^2}{k^2E^3}(k_x+k_y-2k) \tag{3.9}$$

Up until now we have worked with the Hamiltonian H_{K_1}, but with the K_1 hidden. The Berry curvature around K_2 is equal, but with opposite sign (figure 3.1) [2]

3.2 Valley-Hall effect

The Hall conductivity σ_{xy} is

$$\sigma_{xy} = \frac{e^2}{\hbar}\int_{\mathbb{R}^2} f[E^+(k)]\Omega_{k_xk_y}^+ + f[E^-(k)]\Omega_{k_xk_y}^-\frac{d^2\mathbf{k}}{2\pi} \tag{3.10}$$

[2] A short proof for it can be the following: If we send $k_y \to -k_y$ we effectively send $H_{K_1} \to H_{K_2}$.
The berry curvature can be written as $\Omega_{k_xk_y} = i\langle\partial_{k_x}n| \wedge |\partial_{k_y}n\rangle$. By sending $k_y \to -k_y$ we have that $\Omega \to -\Omega$.

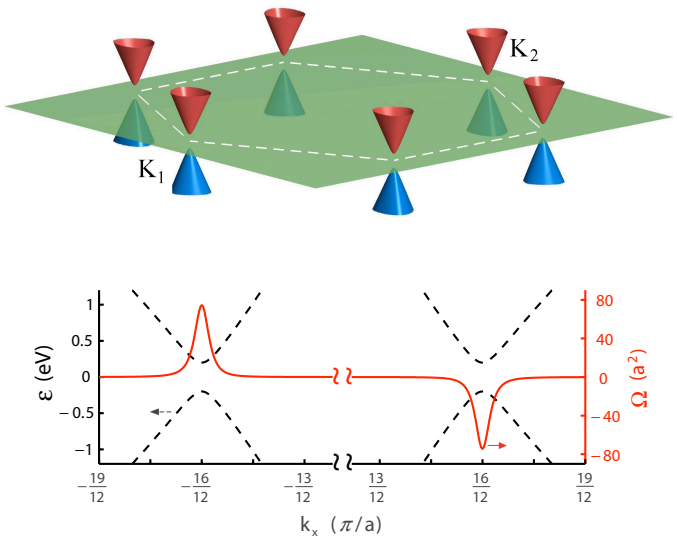

Figure 3.1: In the top panel are displayed the Energy bands in 2D. In the bottom panel with the dotted line are displayed a section of the energy bands, and with the continuous red line the Berry curvature.

Where $f(E) = \left[e^{\beta(E-\mu)} + 1\right]^{-1}$ is the Fermi-Dirac distribution, it is applied once for the states with positive energy and once for the states with negative energy.

We are going to analyze the system at low temperatures ($k_\beta T \ll 1$), so our Fermi-Dirac distribution can be considered like a step-function.

First let's integrate the conductivity for the positive energies and drop the + sign to make the notation lighter.

$$\int_{\mathbb{R}^2} f[E(k)]\Omega_{k_x k_y} dk_x dk_y = \int_{\mathbb{R}^2} f[E(q)]\Omega_{q_x q_y} dq_x dq_y \approx$$

$$\approx \int_0^{2\pi} \int_0^{q_F} \frac{1}{2} \frac{\Delta^2}{q^2 E^3} (q_x + q_y - 2q) q dq d\theta =$$

$$= -2\pi\Delta^2 \int_0^{q_f} \frac{dq}{E^2} = -2\pi\Delta^2 \int_0^{q_f} \frac{dq}{(\Delta^2 + q^2)^{3/2}} = -\frac{2\pi q_F}{\sqrt{\Delta^2 + q_F^2}}$$

And now we express it in terms of the chemical potential μ [3]

$$\int_{\mathbb{R}^2} f[E(k)]\Omega_{k_x k_y} dk_x dk_y \approx -2\pi \frac{\sqrt{\mu^2 - \Delta^2}}{\mu} \theta(\mu - \Delta) \tag{3.11}$$

[3]Here we can use interchangeably μ and E_F

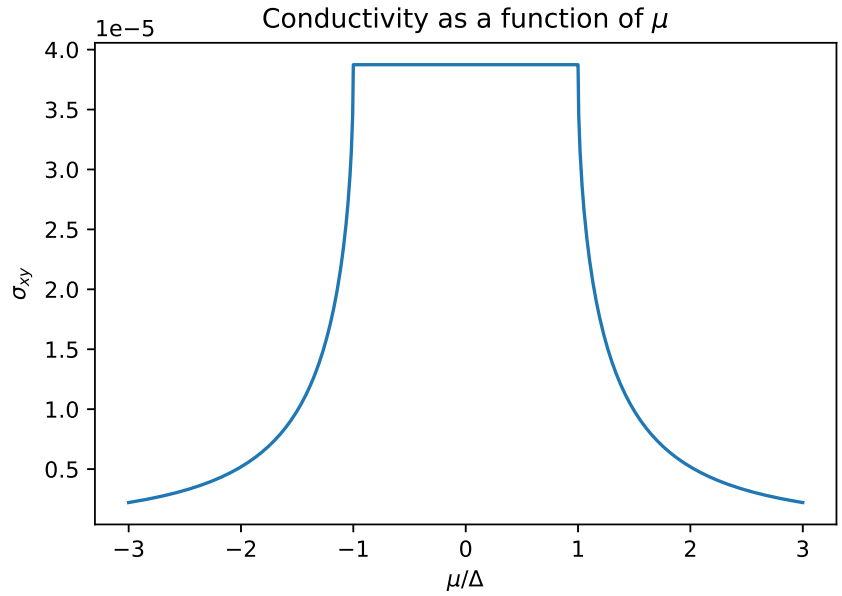

Figure 3.2: Here is shown $\sigma_{xy}(\mu)$ (eq. 3.12). Notice how, when $\mu \in [-\Delta, \Delta]$ then $\sigma_{xy} = \frac{e^2}{2\pi\hbar}$

The $\theta(\mu - \Delta)$ is there to make sure that if no states are inside the Fermi-Dirac the integral is zero. One thing to notice is that if you have $\mu \gg \Delta$ (aka. all states in the band are occupied) then the integral is equal to -2π. The integral of the lower band is very similar. By the end equation of the conductivity 3.10 becomes

$$\sigma_{xy}(\mu) = -\frac{e^2}{2\pi\hbar}\left[\frac{\sqrt{\mu^2 - \Delta^2}}{\mu}\theta(\mu^2 - \Delta^2) - \theta(\mu - \Delta)\right] \tag{3.12}$$

To be fear we only calculated σ_{xy} for the electrons in the valley K_1, the conductivity for the other valley is just $-\sigma_{xy}$. So, putting it all together, we have

$$\sigma_{K_i,xy}(\mu) = (-1)^i\frac{e^2}{2\pi\hbar}\left[\frac{\sqrt{\mu^2 - \Delta^2}}{\mu}\theta(\mu^2 - \Delta^2) - \theta(\mu - \Delta)\right] \tag{3.13}$$

However in most cases it's safe to assume that the chemical potential is inside the energy gap, so equation 3.13 becomes

$$\sigma_{K_i,xy} = (-1)^{i+1}\frac{e^2}{2\pi\hbar} \tag{3.14}$$

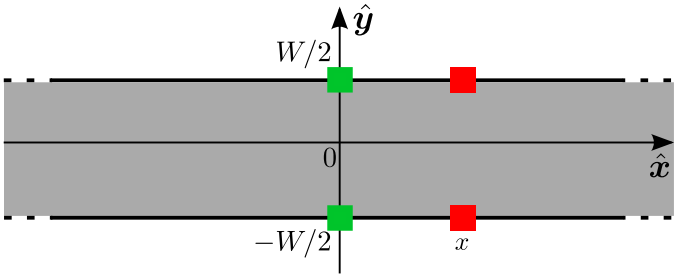

Figure 3.3: Representation of the strip

3.3 Non-local Charge transport

If we apply a voltage V in two opposite points of a strip of a ohmic material of width W and infinite lenght, and we see a current that flows from one point to another figure 3.3.

Clearly the current isn't completely localized along the axis that unites the two injection points, and so does the voltage difference.

If we probe the voltage from two different points with an offset of x from the injection points and we divide it by the total current between the contacts we see that

$$\frac{V(x)}{I} = \frac{2\rho}{\pi} \ln \left| \coth\left(\frac{\pi x}{2W}\right) \right| \tag{3.15}$$

Where ρ is the resistivity. Don't worry later on there is the proof of this equation.

However, two-dimentional material like gapped graphene [6–8] and transition metal dichalcogenides [9–11], don't obey this equation. This is because theese materials display the Valley Hall effect we talked about previously (inserire reference a sezione).

Non-local transport can be a useful tool to probe the existance of anomalous Hall effect [12–17]

3.4 Theory of non local charge transport

The charges inside the material get pushed around from the electrochemical potential ψ_K

$$\psi_K(\mathbf{r}) = V(\mathbf{r}) - \frac{1}{e}\mu_K[n_{K_1}(\mathbf{r}), n_{K_2}(\mathbf{r}), T] \tag{3.16}$$

Where ϕ is the electrical potential, and $\mu_K = \frac{\partial}{\partial n_K} F[n_{K_1}(\mathbf{r}), n_{K_2}(\mathbf{r}), T]$ is the chemical potential of the material and F is the free energy.

The current generated from this potential in the valley K_α in the $i-$th direction is

$$-eJ_{K_\alpha,i}(\mathbf{r}) = \sum_{j,b} \underbrace{-\sigma_{K_\alpha K_\beta,ij}}_{\text{conductivity}} \partial_j \psi_{K_\beta}(\mathbf{r}) \tag{3.17}$$

From now we are going to set $T \approx 0$[4] and ignore intervalley scattering, so if $K_\alpha \neq K_\beta$ $\sigma_{K_\alpha K_\beta,ij} = 0$, also because of this the free energy can be written as the sum of the two Free energies

$$F(n_{K_1}, n_{K_2}) = F_1(n_{K_1}(\mathbf{r})) + F_2(n_{K_2}(\mathbf{r})) \tag{3.18}$$

And so the chemical potential of a given valley depend only on the number of electron in the same valley

$$\mu_\alpha(n_{K_\alpha}(\mathbf{r})) = \frac{\partial}{\partial n_{K_\alpha}} F(n_{K_0}, n_{K_1}) = \frac{\partial}{\partial n_{K_\alpha}} F_\alpha(n_{K_\alpha}(\mathbf{r})) \tag{3.19}$$

This simplifies the trasport equation in

$$-e\mathbf{J}_{K_\alpha}(\mathbf{r}) = \sigma_{K_\alpha}(\mathbf{r}) \nabla \psi_{K_\alpha}(\mathbf{r}) \tag{3.20}$$

Where σ_{K_α} is the following matrix

$$\sigma_{K_\alpha} = \begin{bmatrix} \sigma_{K_\alpha K_\alpha,xx} & \sigma_{K_\alpha K_\alpha,xy} \\ -\sigma^*_{K_\alpha K_\alpha,xy} & \sigma_{K_\alpha K_\alpha,xx} \end{bmatrix}$$

Now we need to write the gradient electrochemical potential $\nabla\psi(\mathbf{r})$

$$\nabla \psi_{K_\alpha}(\mathbf{r}) = \nabla V(\mathbf{r}) - \frac{1}{e} \frac{\partial}{\partial n_{K_\alpha}} \mu_\alpha(n_{K_\alpha}(\mathbf{r})) \nabla n_{K_\alpha} \tag{3.21}$$

From equation INSERIRE REFERENCE A EQUAZIONE we can write for gapped Dirac hamiltonians that VERIFICARE SE VALE ANCHE PER BILAYER GRAPHENE

$$\frac{\partial \mu_{K_\alpha}}{\partial n_{K_\alpha}} = \frac{\pi}{\sqrt{2\pi|n| + \Delta^2}} + \Delta\delta(n) \approx \frac{\pi}{\Delta} + \Delta\delta(n) \quad \forall\alpha$$

In this equation we assumed that there are very few charge carries, so $\frac{n}{\Delta^2} \approx 0$. We can shorten the equation 3.21 by defining

$$e^2 D_{K_\alpha,ij} = \sigma_{K_\alpha,ij} \frac{\partial \mu_\alpha}{\partial n_{K_\alpha}} [n_{K_\alpha}(\mathbf{r})] \tag{3.22}$$

[4] A more precise statement is that the thermal De Broglie wavelenght λ_T must be much larger than the average distance between the electrons. We are not going into the math here, but if you want to calculate it, keep in mind that the dispersion relation is relativistic, so the formula of λ_T is going to be a bit different

So equation 3.20 becomes

$$-eJ_{K_\alpha,i}(\mathbf{r}) = \sigma_{K_\alpha,ij}E_j(\mathbf{r}) - eD_{K_\alpha,ij}\partial_j n_{K_\alpha}(\mathbf{r}) \tag{3.23}$$

or, written in matrix form

$$-e\mathbf{J}_{K_\alpha}(\mathbf{r}) = \sigma_{K_\alpha}\mathbf{E}(\mathbf{r}) - eD_{K_\alpha}\nabla n_{K_\alpha}(\mathbf{r}) \tag{3.24}$$

Where σ_{K_α} and $-eD_{K_\alpha}$ are matrices.

3.4.1 Re-writing the equations in terms of charge current and valley current

Measuring the currents in different valley can be cumbersome, however measuring the charge current $\mathbf{J}_c = \mathbf{J}_{K_1} + \mathbf{J}_{K_2}$ is straightforward, and for mathematical convenience we also define the valley current $\mathbf{J}_v = \mathbf{J}_{K_1} - \mathbf{J}_{K_2}$.

Since we no longer describe the currents in terms of their valley index, but on the sum and the difference of what happens at the different valleys, we are going to reparametrize also the other quantities in the same fashion.

$$\begin{cases} \sigma_c = \sigma_{K_1} + \sigma_{K_2} = 2\sigma_{xx}\delta_{ij} \\ \sigma_v = \sigma_{K_1} - \sigma_{K_2} = \sigma_v = 2\sigma_{xy}\epsilon_{ij} \end{cases} \tag{3.25}$$

The term $-eD_{K_\alpha}\nabla n_{K_\alpha}(\mathbf{r})$ is a little harder to traslate. First off we are going to impose the local charge conservation

$$n(\mathbf{r}) = n_{K_0} + n_{K_1} \approx 0$$

and so

$$n_v(\mathbf{r}) = n_{K_1} - n_{K_2} = 2n_{K_1} = -2n_{K_2} \tag{3.26}$$

Now let's do the sum of the $D_{K_\alpha}\nabla n_{K_\alpha}(\mathbf{r})$ terms to write them in terms of charge and valleys degrees of freedom

$$D_{K_1}\nabla n_{K_1} + D_{K_2}\nabla n_{K_2} = (D_{K_1} - D_{K_2})\nabla n_v(\mathbf{r})/2$$

$$D_{K_1} - D_{K_2} = \sigma\frac{\partial\mu_1}{\partial n_{K_1}} - \sigma^T\frac{\partial\mu_2}{\partial n_{K_2}}$$

since $\mu_v = 2\mu_1 = -2\mu_2$ and $n_v = 2n_{K_1} = -2n_{K_2}$

$$D_{K_1} - D_{K_2} = \frac{1}{e^2}(\sigma - \sigma^T)\frac{\partial\mu_v}{\partial n_v} = \frac{2}{e^2}\sigma_v\frac{\partial\mu_v}{\partial n_v}$$

so I define

$$D_{cv} = \frac{2}{e^2}\sigma_v\frac{\partial\mu_v}{\partial n_v} \approx \frac{2}{e^2}\frac{\pi}{\Delta}\sigma_v$$

so we get that

$$D_{K_1}\nabla n_{K_1} + D_{K_2}\nabla n_{K_2} = D_{cv} n_v$$

Putting it all together we have that

$$\mathbf{J}_c(\mathbf{r}) = \sigma_c \mathbf{E}(\mathbf{r}) + eD_{cv}\nabla n_v(\mathbf{r})$$

Writing all the indices

$$J_{c,i} = \sum_j \sigma_{c,xx}\delta_{ij}E_i + D_{cv,xy}\epsilon_{ij}\partial_j n_v \tag{3.27}$$

so we can rewrite them as

$$\mathbf{J}_c = \sigma_{c,xx}\mathbf{E}_i + D_{cv,xy}\nabla \times n_v \tag{3.28}$$

where $\sigma_{c,xx}$ and $D_{cv,xy}$ are scalars.

And now the difference of the $D_{K_\alpha}\nabla n_{K_\alpha}(\mathbf{r})$ terms to write them in terms of charge and valleys degrees of freedom

$$D_{K_0}\nabla n_{K_0} - D_{K_1}\nabla n_{K_1} = (D_{K_0} + D_{K_1})\nabla n_v(\mathbf{r})/2$$

and with some calculations done in a similar fashion to the one we use to calculate $\mathbf{J}_c$ we have that

$$D_v = \frac{1}{2}(D_{K_0} + D_{K_1}) = \frac{1}{e^2}\sigma_c \frac{\partial \mu_c}{\partial n_c}$$

so, in matrix form

$$\mathbf{J}_v(\mathbf{r}) = \sigma_v \mathbf{E}(\mathbf{r}) + eD_v \nabla n_v(\mathbf{r}) \tag{3.29}$$

which can be re-written as

$$J_{v,i}(\mathbf{r}) = \sum_j \sigma_{c,xy}\epsilon_{ij}E_j(\mathbf{r}) + eD_{v,xx}\delta_{ij}\partial_j n_v(\mathbf{r}) \tag{3.30}$$

where $\sigma_{c,xy}$ and $D_{v,xx}$ are scalars

3.4.2 Laplace equation

Now that we have the charge and valley currents differential equations we calculate the laplacians to solve them. Let's start from the equation for the charge currents 3.28

$$\nabla \cdot \mathbf{J}_c = \nabla \cdot (\sigma_c \mathbf{E}) + eD_{cv,xx}\nabla \cdot (\nabla \times n_v) \tag{3.31}$$

Inside the material the are no sources of charge current, so $\nabla \cdot \mathbf{J}_c =$, and the divergence of a rotor is zero, so $\nabla \cdot (\nabla \times n_v) = 0$. This means that inside the material

$$\boxed{\nabla^2 V(x,y) = 0} \tag{3.32}$$

So, to be able to solve the laplace equation we just need to impose the boundary conditions that the current is injected in a single point at $x = 0$ along the $\hat{\mathbf{y}}$ direction.

$$-e\mathbf{J}_c(x, \pm W/2) = I\delta(x)\hat{\mathbf{y}}$$

If we put it in equation 3.31 we get

$$\boxed{I\delta(x) = \sigma_{c,xx}\partial_y V(x, \pm W/2) - eD_{cv,xy}\partial_x n_v(x, \pm W/2)} \tag{3.33}$$

Now let's calculate the laplacian for the valley current equation 3.30

$$\nabla \cdot \mathbf{J}_v = \nabla \times (\sigma_{c,xy}\mathbf{E}) + e\nabla \cdot (D_{v,xx}\nabla n_v) \tag{3.34}$$

Now, lets analyze all the terms one by one

- For the continuity equation we have that $\nabla \cdot \mathbf{J}_v = \frac{\partial}{\partial t} n_v$, since intervalley scattering is zero, this should be zero, but why don't add it back now? so we say that it decays exponentially $\frac{\partial}{\partial t} n_v = -\frac{1}{\tau_v} n_v$
- $e\nabla \cdot (D_{v,xx}\nabla n_v)$ is really nothing special, inside the material $D_{v,xx}$ is constsant so in the end it is equal to $eD_{v,xx}\nabla^2 n_v$
- $\nabla \times (\sigma_{c,xy}\mathbf{E})$ is equal to zero inside the material, but on the edge can be non-zero because $\sigma_{c,xy}$ changes form inside to the outside

In the end we get that

$$eD_{v,xx}\nabla^2 n_v = -\frac{1}{\tau_v} n_v - \nabla \times (\sigma_{c,xy}\mathbf{E}) \tag{3.35}$$

This means that at the equilibrium $n_v \neq 0$ only if you are were $\nabla \times (\sigma_{c,xy}\mathbf{E}) \neq 0$, and this is only true along the edge, so we we'll have to worry about this term only in the boundary conditions, So

$$\boxed{\left[\nabla^2 - \frac{1}{\tau_v D_{v,xx}}\right] n_v(\mathbf{r}) = 0} \tag{3.36}$$

The boundary condition is simply that the valley current doesn't exit the material, so

$$J_{v,y}(x, \pm W/2) = 0 \tag{3.37}$$

putting it into the differential equation for J_v (eq 3.30) we get

$$\boxed{\sigma_{v,xy}\partial_x V(x, \pm W/2) + eD_{v,xx}\partial_y n_v(x, \pm W/2) = 0} \tag{3.38}$$

All the boxed equations we wrote in the in this section enable us to completely solve the system. For convenience let's write the m in a single system of equations

$$\begin{cases} \nabla^2 V(x,y) = 0 \\ \left[\nabla^2 - \frac{1}{\tau_v D_{v,xx}}\right] n_v(\mathbf{r}) = 0 \\ I\delta(x) = \sigma_{c,xx}\partial_y V(x, \pm W/2) - eD_{cv,xy}\partial_x n_v(x, \pm W/2) \\ \sigma_{v,xy}\partial_x V(x, \pm W/2) + eD_{v,xx}\partial_y n_v(x, \pm W/2) = 0 \end{cases} \tag{3.39}$$

From the third equation in the system above we can see that $V(x,y)$ is even along the $\hat{\mathbf{x}}$ axis and odd along the $\hat{\mathbf{y}}$ axis.
From the fourth equation we can see that n_v has the opposite parity to V, so it's odd along the $\hat{\mathbf{x}}$ axis and even along the $\hat{\mathbf{y}}$ axis.

To be able to solve it we first have to do a fourier transform over the $\hat{\mathbf{x}}$ direction. The first two equations of eq 3.39 become

$$\begin{cases} (\partial_y^2 - k^2)V(k,y) = 0 \\ \left[\partial_y^2 - \omega^2(k)\right] n_v(k,y) = 0 \end{cases} \tag{3.40}$$

And the solutions that respect the symmetries we talked about earlier are

$$V(k,y) = V(k)\sinh(ky) \qquad n_v(k,y) = n_v(k)\cosh[\omega(k)y] \tag{3.41}$$

However we still don't know what are $V(k)$ and $n_v(k)$, to obtain them we have to plug the equations above in the last two equations of 3.39

$$\begin{cases} \sigma_{c,xx} k \cosh(kw/2)V(k) - eD_{cv,xy} ik \cosh(\omega W/2) n_v(k) = I \\ -\sigma_{v,xy} ik \sinh(kw/2)V(k) - eD_{v,xx}\omega(k)\sinh(\omega W/2) n_v(k) = 0 \end{cases} \tag{3.42}$$

This system of equation is linear in $V(k)$ and $n_v(k)$, so it can be written in this form

$$\begin{bmatrix} A & B \\ C & D \end{bmatrix} \begin{bmatrix} V \\ n_v \end{bmatrix} = \begin{bmatrix} I \\ 0 \end{bmatrix} \tag{3.43}$$

And the inverse is simply

$$\begin{bmatrix} V \\ n_v \end{bmatrix} = \frac{I}{AD - BC} \begin{bmatrix} D \\ -C \end{bmatrix} \tag{3.44}$$

Since we want only care to calculate the voltage we only need to evaluate

$$V = \frac{I}{A - \frac{BC}{D}}$$

wich turns out to be equal to

$$V(k) = \frac{I}{\sigma_c} \frac{\omega(k)/k}{\sinh(kW/2)} \left\{ \frac{\omega(k)}{\tanh(kW/2)} + \frac{k \tan^2(\theta_{VH})}{\tanh[\omega(k)W/2]} \right\}^{-1} \tag{3.45}$$

We can plug it into equation 3.41 and evaluate it at $y = \pm W/2$

$$V(k, \pm W/2) = V(k) \sinh(\pm kW/2) = \frac{I\omega}{\sigma_c k} \left\{ \dots \right\}^{-1} \tag{3.46}$$

Where the terms inside the curly brakets are the same from the previous equation (3.45).
Finally we can calculate the non-local resistance

$$R_{NL}(k) = \frac{V(k, W/2) - V(k, -W/2)}{I} \tag{3.47}$$

Which is equal to

$$R_{NL}(k) = \frac{2\omega(k)}{k\sigma_c} \left\{ \frac{\omega(k)}{\tanh(kW/2)} + \frac{k \tan^2(\theta_{VH})}{\tanh[\omega(k)W/2]} \right\}^{-1} \tag{3.48}$$

Chapter 4

Study of R_{NL}

Let's from the frequency response of the non-local response that we talked about in section **??** [18]

$$R_{\mathrm{NL}}(k) = \frac{2\omega(k)}{k\sigma_c}\left\{\frac{\omega(k)}{\tanh(kW/2)} + \frac{k\tan^2(\theta_{\mathrm{VH}})}{\tanh[\omega(k)W/2]}\right\}^{-1} \tag{4.1}$$

Its anti-fourier transform tells us everything we would want to know about the system. Unfortunately 4.1 doesn't have an analytic Fourier transform. If there are no topological effect $\theta_{\mathrm{VH}} = 0$ and it can be solved analytically.

$$R_{\mathrm{NL}}(k)|_{\theta_{\mathrm{VH}}=0} \equiv R^{(0)}_{\mathrm{NL}}(k) = \frac{2\rho}{k}\tanh\left(\frac{kW}{2}\right) \tag{4.2}$$

$$R^{(0)}_{\mathrm{NL}}(x) = \mathcal{F}^{-1}\left[R^{(0)}_{\mathrm{NL}}(k)\right] = -\frac{2\rho}{\pi}\ln\left|\tanh\left(\frac{\pi x}{2W}\right)\right| \tag{4.3}$$

This is the purely ohmic nonlocal signal that we have talked about in 3.15. However, if we are going to explore topological materials we cannot set $\tan(\theta_{\mathrm{VH}}) = 0$, this means that we'll have to do some approximations.

4.1 Study of $R_{\mathrm{NL}}(x)$

Let's look at the graph of the $R_{\mathrm{NL}}(k)$ before doing any approximations: As you can see from the figure 4.1

- If $W \gg l_{\mathrm{v}}$ we have a single bell like function with the width of the bell being $\approx 1/W$ and the height being R_{xx}
- If $W \ll l_{\mathrm{v}}$ we have a double-bell function, where the first bell has a height of R_{xx} and a width of $\approx 1/l_{\mathrm{v}}$, and the second one has a shorter height.

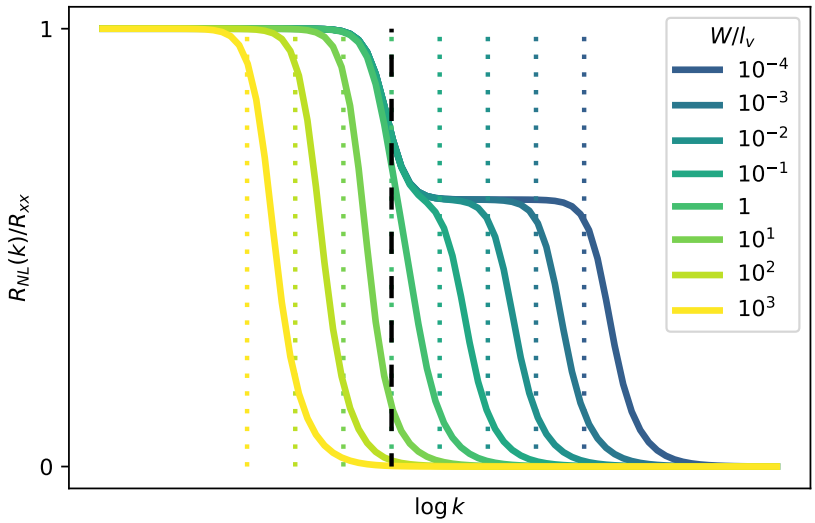

Figure 4.1: $R_{NK}(k)$ for several values of W/l_{v}. The dashed black line represents where $k = 1/l_{\mathrm{v}}$, the colored dashed line represents where $k = 1/W$

To evaluate the precise height of the secondary bell we just need to set $l_{\mathrm{v}}^{-1} \ll k \ll W^{-1}$ in equation 4.1, this gives us

$$R_{\mathrm{NL}}(l_{\mathrm{v}}^{-1} \ll k \ll W^{-1}) \approx R_{xx} \cos^2(\theta_{\mathrm{VH}}) \tag{4.4}$$

Where $R_{xx} = \frac{W}{\sigma_{xx}}$ and $\cos^2(\theta_{\mathrm{VH}}) = \frac{1}{1+\tan^2(\theta_{\mathrm{VH}})}$

So, if we have $l_{\mathrm{v}} \ll W$ or $\theta_{\mathrm{VH}} \ll 1$ (or both) we have a single bell structure. Incidentally these are the conditions to NOT have topological effects, so the less visible the double bell is, the less visible the topological effects are. We'll also see later how one of the bell represents the ohmic nonlocal signal, while the other represents the topological nonlocal signal.

4.1.1 Small k

Let's start by exploring $k \ll l_{\mathrm{v}}^{-1}, W^{-1}$. This will tell us how the function behaves at long ranges $x \gg l_{\mathrm{v}}, W$. In this regime

$$\omega(k) = \sqrt{k^2 + l_{\mathrm{v}}^{-2}} \approx \frac{1}{l_{\mathrm{v}}}\left[1 + \frac{(kl_{\mathrm{v}})^2}{2}\right] \tag{4.5}$$

$$\coth(kW/2) \approx \frac{2}{kW} + \frac{kW}{6} \tag{4.6}$$

Plugging the last two equations into equation 4.1 we have that $R_{\mathrm{NL}}(k) \approx$

$$\frac{2}{\sigma_c}\frac{1}{l_{\mathrm{v}}k}\left[\frac{1}{l_{\mathrm{v}}}\left(1+\frac{k^2 l_{\mathrm{v}}^2}{2}\right)\left(\frac{2}{kW}+\frac{kW}{6}\right)+\frac{k\tan^2(\theta_{\mathrm{VH}})}{\tanh(W/2l_{\mathrm{v}})}+o(k^2)\right]^{-1} \tag{4.7}$$

And after some steps we get that

$$R_{\mathrm{NL}}(k \ll l_{\mathrm{v}}^{-1}, W^{-1}) = \frac{R_{xx}}{1+L_{\mathrm{v}}^2 k^2 + o(k^4)} \tag{4.8}$$

Where the *renormalized valley diffusion length* L_{v}^2 is defined as

$$L_{\mathrm{v}}^2 \equiv l_{\mathrm{v}}^2 + \frac{W^2}{12} + \frac{l_{\mathrm{v}}W}{2}\frac{\tan^2(\theta_{\mathrm{VH}})}{\tanh(W/2l_{\mathrm{v}})} \tag{4.9}$$

Now we are going to define the topological nonlocal resistance R_{NL}^T by taking the equation 4.8, and ignoring the $o(k^4)$ term

$$R_{\mathrm{NL}}^T(k) \equiv \frac{R_{xx}}{1+L_{\mathrm{v}}^2 k^2} \tag{4.10}$$

We are now ready to do the Fourier transform of equation 4.10 to get the behavior for $x \gg l_{\mathrm{v}}, W$

$$R_{\mathrm{NL}}(x \gg l_{\mathrm{v}}, W) \approx \mathcal{F}^{-1}\left[R_{\mathrm{NL}}^T(k)\right] \equiv R_{\mathrm{NL}}^T(x) \tag{4.11}$$

That is equal to

$$R_{\mathrm{NL}}^T(x) = R_{xx}\int_{-\infty}^{+\infty}\frac{e^{-ikx}}{1+L_{\mathrm{v}}^2k^2}\frac{dk}{2\pi} = \frac{R_{xx}}{2L_{\mathrm{v}}}e^{-\frac{|x|}{L_{\mathrm{v}}}} \tag{4.12}$$

So,

$$R_{\mathrm{NL}}(x \gg l_{\mathrm{v}}, W) \approx R_{\mathrm{NL}}^T(x) \tag{4.13}$$

4.1.2 Big k

Fortunately the case for which $k \gg l_{\mathrm{v}}^{-1}$ is much simpler: in this case $\omega(k) \approx k$, so

$$R_{\mathrm{NL}}(k \gg l_{\mathrm{v}}^{-1}) = \cos^2(\theta_{\mathrm{VH}})\frac{2\rho}{k}\tanh\left(\frac{kW}{2}\right) \tag{4.14}$$

Using equation 4.2 we get that this last equation is $\cos^2(\theta_{\mathrm{VH}})$ times the one for the purely ohmic nonlocal signal

$$R_{\mathrm{NL}}(k \gg l_{\mathrm{v}}^{-1}) \approx \cos^2(\theta_{\mathrm{VH}})R_{\mathrm{NL}}^{(0)}(k) \tag{4.15}$$

This means that the Fourier transform is

$$R_{\mathrm{NL}}(x \ll l_{\mathrm{v}}) \approx \cos^2(\theta_{\mathrm{VH}})R_{\mathrm{NL}}^{(0)}(x) \tag{4.16}$$

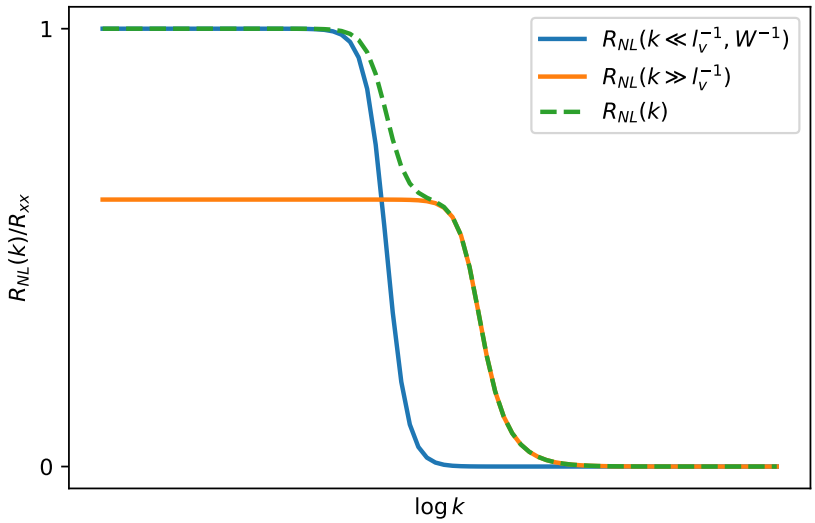

Figure 4.2: For this example $l_\mathrm{v} = 20W$

4.1.3 Testing the approximations

But how do these equations fear in practice? As you can see from figure 4.2 the two approximations work pretty well, except in the neighborhood where $k \approx l_\mathrm{v}^{-1}$. But what we really care about is $R_\mathrm{NL}(x)$.
If we plot the approximations for $x \gg l_\mathrm{v}, W$ (eq. 4.13) and $x \ll l_\mathrm{v}$ (eq. 4.16) alongside the numerical Fourier transform of $R_\mathrm{NL}(k)$ 4.1 we get figure 4.3

4.1.4 Improving the approximation

We can do better than this! By combining the two approximations it's possible to have a single equation that is very accurate for both $x \gg l_\mathrm{v}, W$ and $x \ll l_\mathrm{v}$, however, in the end we'll end up with an approximation that is surprisingly good even for $x \approx l_\mathrm{v}$.

Since the Fourier transform is a linear operator, the idea is to find the linear combination of the two approximation that best approximates the $R_\mathrm{NL}(k)$ for both $k \ll l_\mathrm{v}^{-1}, W^{-1}$ and $k \gg l_\mathrm{v}^{-1}$ and then anti-transform the result.

$$R_\mathrm{NL}(k) \approx \alpha R_\mathrm{NL}(k \ll l_\mathrm{v}^{-1}, W^{-1}) + \beta R_\mathrm{NL}(k \gg l_\mathrm{v}^{-1}) =$$

$$= R_\mathrm{NL}(k) \approx \alpha R^T_\mathrm{NL}(k) + \beta \cos^2(\theta_\mathrm{VH}) R^{(0)}_\mathrm{NL}(k)$$

Where α and β are the coefficient to be determined.
Since we only need to evaluate two variables, we only need to evaluate the

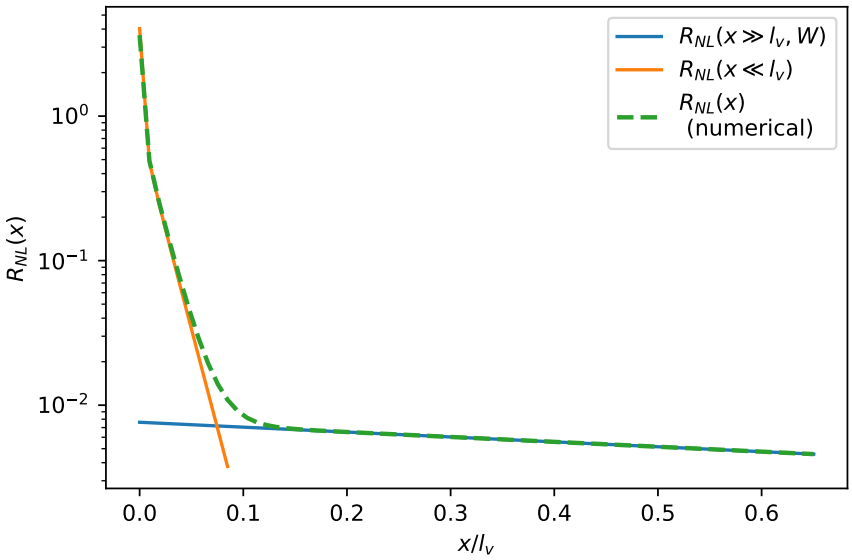

Figure 4.3: The parameters for this graph are exactly the same for the previous graph (figure 4.2)

expression above in two different points. The most reasonable points to choose are $k = 0$ and $k = +\infty$, since they are the points where the approximations work better. For doing the calculations it's best to write out the two approximations

$$R_{\mathrm{NL}}(k) \approx \alpha \frac{R_{xx}}{1 + L_{\mathrm{v}}^2 k^2} + \beta \frac{2\rho}{k} \tanh\left(\frac{kW}{2}\right) \cos^2(\theta_{\mathrm{VH}})$$

- For $k \to +\infty$ the term that is multiplied by β is an increasingly precise estimate of $R_{\mathrm{NL}}(k)$, and it dominates over the term that is multiplied by alpha, so $\beta = 1$.
- For $k = 0$ we have that

  $$R_{xx} = \alpha R_{xx} + R_{xx} \cos^2(\theta_{\mathrm{VH}})$$

  So, $\alpha = \sin^2(\theta_{\mathrm{VH}})$.

Putting it all together we define the resulting approximation

$$\boxed{\tilde{R}_{\mathrm{NL}}(k) \equiv \sin^2(\theta_{\mathrm{VH}}) R_{\mathrm{NL}}^{T}(k) + \cos^2(\theta_{\mathrm{VH}}) R_{\mathrm{NL}}^{(0)}(k)} \tag{4.17}$$

The thing that I personally like about this approximation is its geometrical elegance. If we write all the terms of the equation above we get

$$\tilde{R}_{\mathrm{NL}}(k) \equiv \sin^2(\theta_{\mathrm{VH}}) \frac{R_{xx}}{1 + L_{\mathrm{v}}^2 k^2} + \cos^2(\theta_{\mathrm{VH}}) \frac{2\rho}{k} \tanh\left(\frac{kW}{2}\right) \tag{4.18}$$

And if we plot the approximation $\tilde{R}_{\mathrm{NL}}(k)$ alongside the actual values of $R_{\mathrm{NL}}(k)$ we can see that they are remarkably similar (figure 4.4)

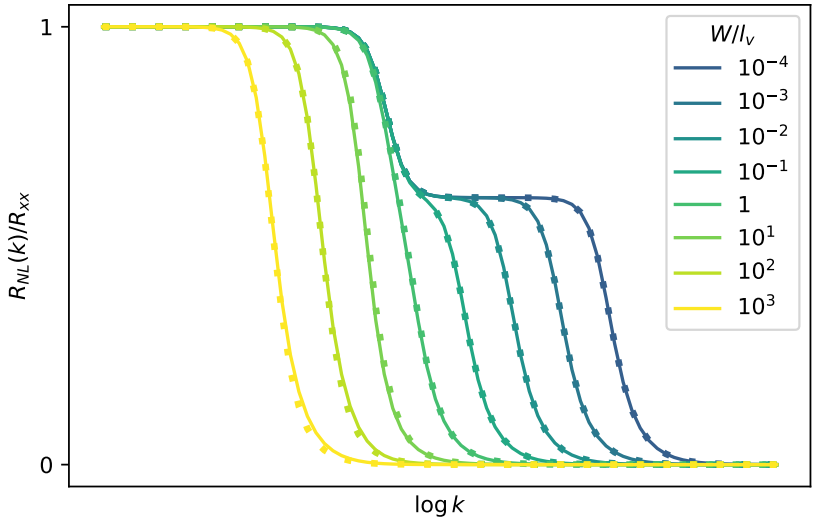

Figure 4.4: Comparison between $R_{\mathrm{NL}}(k)$ and $\tilde{R}_{\mathrm{NL}}(k)$. The continuous line represents $R_{\mathrm{NL}}(k)$, while the dashed line represents $\tilde{R}_{\mathrm{NL}}(k)$. It's unreasonably accurate!

The nice thing about this is that if two equations are similar, then their Fourier transform will be too. This means that $\tilde{R}_{\mathrm{NL}}(x)$ will be a good approximation of $R_{\mathrm{NL}}(x)$, where

$$\boxed{\tilde{R}_{\mathrm{NL}}(x) = \sin^2(\theta_{\mathrm{VH}}) R^T_{\mathrm{NL}}(x) + \cos^2(\theta_{\mathrm{VH}}) R^{(0)}_{\mathrm{NL}}(x)} \tag{4.19}$$

We can write out the full formula using equations 4.13 and 4.16

$$\tilde{R}_{\mathrm{NL}}(x) = \frac{R_{xx}}{2L_{\mathrm{v}}} e^{-|x|/L_{\mathrm{v}}} \sin^2(\theta_{\mathrm{VH}}) - \frac{2R_{xx}}{\pi W} \ln \left| \tanh\left(\frac{\pi x}{2W}\right) \right| \cos^2(\theta_{\mathrm{VH}}) \tag{4.20}$$

Infact if we re-create figure 4.3 with the equation above we get figure 4.5

4.2 $R_{\mathrm{NL}}(x)$ as we change ρ

Hall effect experiments are generally done in Hall-bars. These are samples of material with a shape like the one in figure 4.6, it also means that more often than not in experimental setups we cannot change x without changing the geometry of the sample.

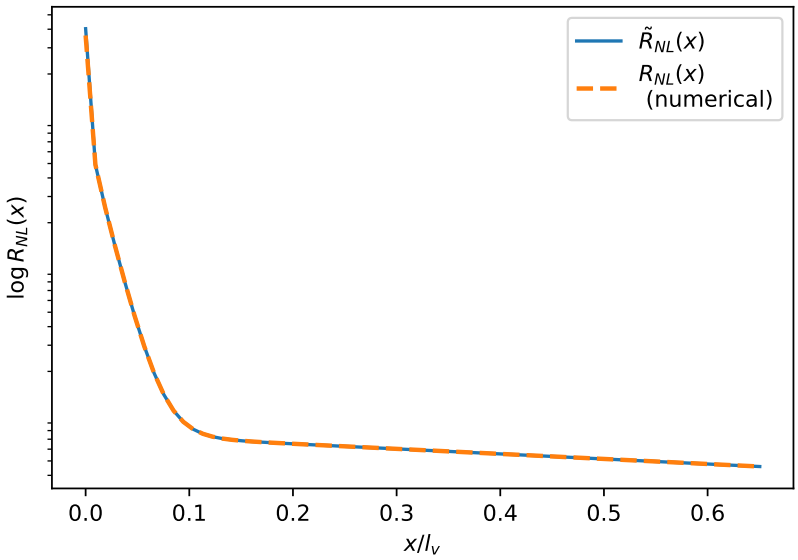

Figure 4.5: As you can see it's impossible to distinguish the difference between the two functions to the naked eye. The parameters are the same as figure 4.5

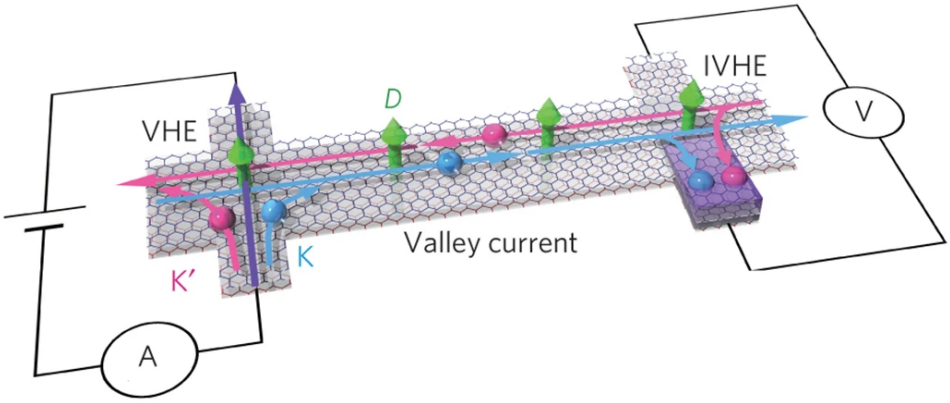

Figure 4.6: Example of Hall bar the currents are injected and measured in the rectangular contacts that come out from the main strip

In the previous section we studied how R_{NL} depended on x, but since Hall-bars can only measure a single x one of the ways to have multiple measurements with the same Hall-bar is to change the resistivity of the material by changing the temperature of the setup, and study R_{NL} as we change ρ_{xx}.

If you were to conduct an experiment where you measure R_{NL} as you

change the resistivity of the material ρ you would have in general something that looks like figure 4.7.

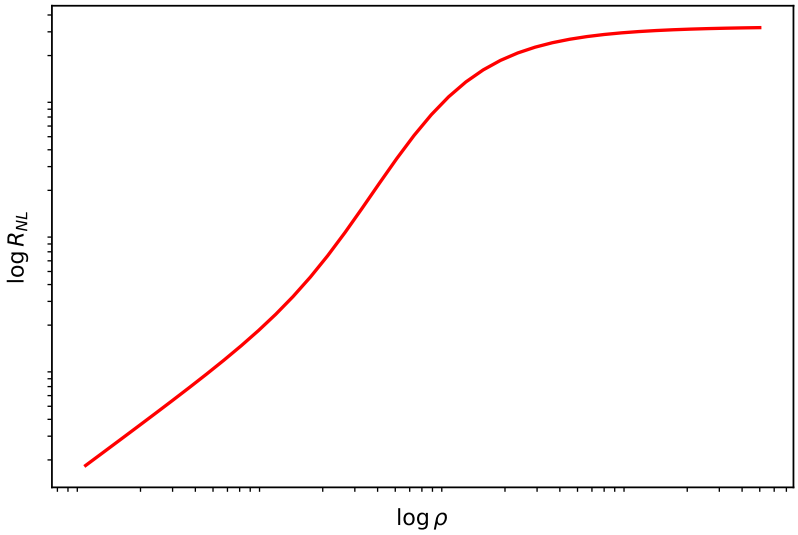

Figure 4.7: Looking at the image you can see that at the start it increases linearly, then it starts to increase even faster just before reaching a plateau.

The objective of this section is effectively to be able to understand this graph.

Just like before to understand the general behavior of $R_{\mathrm{NL}}(\rho)$ we'll examine $\rho \to 0$ and $\rho \to \infty$. For convenience let's re-write equation 4.1

$$R_{\mathrm{NL}}(k) = \frac{2\omega(k)}{k\sigma_c}\left\{\frac{\omega(k)}{\tanh(kW/2)} + \frac{k\tan^2(\theta_{\mathrm{VH}})}{\tanh[\omega(k)W/2]}\right\}^{-1}$$

4.2.1 Low resistivities $\rho \to 0$

Sending $\rho \to 0$ is effectively equal to sending $\tan(\theta_{\mathrm{VH}}) = \sigma_{\mathrm{v}}\rho \to 0$. To be more precise we are going to assume that

$$\frac{k\tan^2(\theta_{\mathrm{VH}})}{\tanh[\omega(k)W/2]} \ll \frac{\omega(k)}{\tanh(kW/2)} \qquad \forall k$$

Which means that $\tan^2(\theta_{\mathrm{VH}}) \ll 1$. So now we do a Taylor series expansion of the above equation around $\tan^2(\theta_{\mathrm{VH}}) = 0$.

$$R_{\mathrm{NL}}(k) \approx R_{\mathrm{NL}}(k)|_{\tan^2(\theta_{\mathrm{VH}})=0} + \frac{\partial}{\partial\tan^2(\theta_{\mathrm{VH}})}R_{\mathrm{NL}}(k)|_{\tan^2(\theta_{\mathrm{VH}})=0}$$

that we are going to re-define as

$$R_{\mathrm{NL}}(k) \approx R^{(0)}_{\mathrm{NL}}(k) + R^{(1)}_{\mathrm{NL}}(k)\tan^2(\theta_{\mathrm{VH}})$$

The zeroth order term gives us our good old ohmic response in the frequency domain (eq. 4.2)

$$R^{(0)}_{\mathrm{NL}}(k) = \frac{2\rho}{k}\tanh\left(\frac{kW}{2}\right)$$

This makes sense because as we lower ρ/ρ_{v} the hall current will be increasingly smaller and so the ohmic response will dominate.
And if we do the Fourier transform to get the x dependent form we get the ohmic nonlocal resistivity 3.15

$$R^{(0)}_{\mathrm{NL}}(x) = \frac{2\rho}{\pi}\ln\left|\coth\left(\frac{\pi x}{2W}\right)\right| \tag{4.21}$$

Now let's calculate the first order term

$$R^{(1)}_{\mathrm{NL}}(k)\tan^2(\theta_{\mathrm{VH}}) = -2\rho\frac{\omega(k)}{k}\left[\frac{\omega(k)}{\tanh(Wk/2)}\right]^{-2} k\frac{\tan^2(\theta_{\mathrm{VH}})}{\tanh(\omega(k)W/2)} =$$

$$= -2\rho^3\sigma_{\mathrm{v}}^2\tanh^2\left(\frac{kW}{2}\right)\left\{\omega(k)\tanh\left[\frac{\omega(k)W}{2}\right]\right\}^{-1} \equiv \rho^3 F(k)$$

where $F(k)$ is defined as follows

$$F(k) \equiv -2\sigma_{\mathrm{v}}^2\tanh^2\left(\frac{kW}{2}\right)\left\{\omega(k)\tanh\left[\frac{\omega(k)W}{2}\right]\right\}^{-1} \tag{4.22}$$

And it doesn't depend on ρ. Its Fourier transform is

$$F(x) = -2\sigma_v^2\int_{-\infty}^{+\infty}\tanh^2\left(\frac{kW}{2}\right)\left\{\tanh\left[\frac{\omega(k)W}{2}\right]\right\}^{-1}\frac{e^{-ikx}}{\omega(k)}\frac{dk}{2\pi} \tag{4.23}$$

Putting it all together we get that

$$\lim_{\rho\to 0} R_{\mathrm{NL}}(x) = \frac{2\rho}{\pi}\ln\left|\coth\left(\frac{\pi x}{2W}\right)\right| + \rho^3 F(x) + o(\rho^5) \tag{4.24}$$

4.2.2 Big resistivities $\rho \to \infty$

Now let's study what happens when $\rho, \tan(\theta_{\mathrm{VH}}) \to \infty$. First off let's rewrite equation 4.1 and bring the $\omega(k)$ and k inside the curly braces.

$$R_{\mathrm{NL}}(k) = 2\rho\Bigg\{\underbrace{\frac{k}{\tanh(kW/2)}}_{\substack{\text{cannot be}\\ \text{ignored for } k=0}} + \frac{k^2}{\omega(k)}\frac{\tan^2(\theta_{\mathrm{VH}})}{\tanh[\omega(k)W/2]}\Bigg\}^{-1} \tag{4.25}$$

This limit is a bit tricky to evaluate. First off even thought the rightmost term inside the curly braces dominates everywhere except for $k = 0$ this "*small detail*" is crucial. From image 4.8 we can see that the larger ρ gets, the smaller the area around $k = 0$ where the first term dominates.

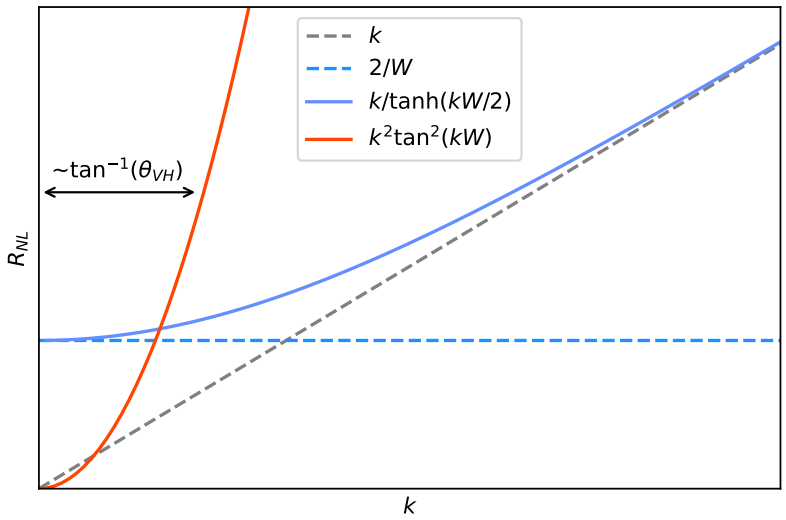

Figure 4.8: This graph shows the elements inside the curly brakets in equation 4.25. The continuous blue line represents the first term, the blue dashed line represents its approximation around $k = 0$ and the gray dashed lines represent its approximation for $k \to \infty$.
The orange parabola represents the right-hand side term $\frac{k^2}{\omega(k)} \frac{\tan^2(\theta_{\mathrm{VH}})}{\tanh[\omega(k)W/2]}$

For high values of $\rho, \tan(\theta_{\mathrm{VH}})$ the parabola becomes really narrow, and it overtakes the first term. This means that for the values of $\tan(\theta_{\mathrm{VH}})$ such that the parabola manages to overtake the $k \tanh^2(kW/2)$ term before $k = 2/W$ we can approximate the first term as being always equal to $2/W$. To be more precise

$$\left(\frac{2}{W}\right)^2 \frac{1}{\omega(2/W)} \frac{\tan^2(\theta_{\mathrm{VH}})}{\tanh[\omega(2/W)W/2]} \gg \frac{2}{W}$$

so,

$$\tan^2(\theta_{\mathrm{VH}}) \gg \sqrt{1 + \frac{W^2}{4l_{\mathrm{v}}^2}} \tanh\left(\sqrt{1 + \frac{W^2}{4l_{\mathrm{v}}^2}}\right) \tag{4.26}$$

This means that in that case

$$R_{\mathrm{NL}}(k) \approx 2\rho\left\{\frac{2}{W} + \frac{k^2}{\omega(k)}\frac{\tan^2(\theta_{\mathrm{VH}})}{\tanh[\omega(k)W/2]}\right\}^{-1} \tag{4.27}$$

Ok, low let's take a look at this function as we make ρ bigger and bigger

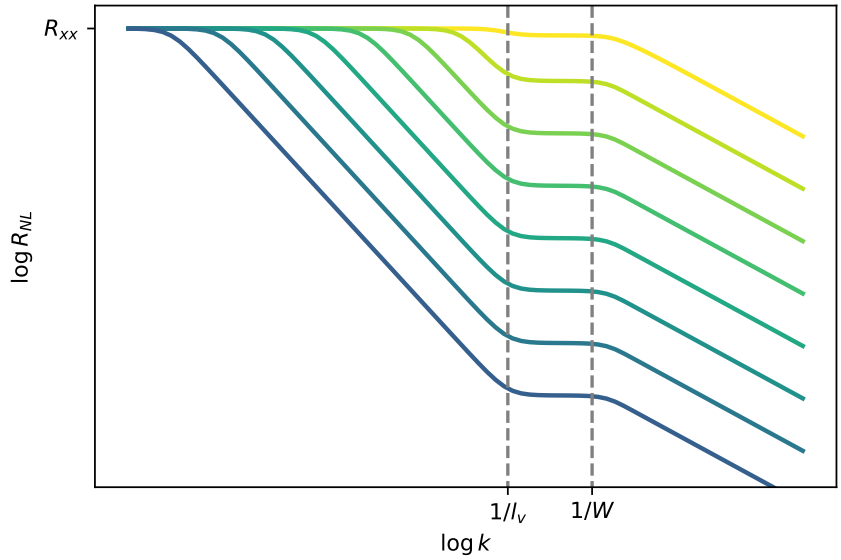

Figure 4.9: In this graph the darker the line color is, the bigger is the value of ρ. Notice how, as we increase ρ the first regime becomes more dominant

As you can see from figure 4.9 are three regimes here. The first one in for $k < l_{\mathrm{v}}^{-1}$, the second one is for $l_{\mathrm{v}}^{-1} < k < W^{-1}$ and the third one is for $W^{-1} < k$

First regime

In the first regime ($k < l_{\mathrm{v}}^{-1}$) $R_{\mathrm{NL}}(k)$ is similar to a Lorentzian function.

$$\lim_{\rho\to\infty} R_{\mathrm{NL}}(k) = 2\rho\left\{\frac{2}{W} + l_{\mathrm{v}}k^2\frac{\tan^2(\theta_{\mathrm{VH}})}{\tanh[W/2l_{\mathrm{v}}]}\right\}^{-1} \tag{4.28}$$

We can re-parametrize it As

$$\lim_{\rho\to\infty} R_{\mathrm{NL}}(k) = \frac{R_{xx}}{1 + (k/\Gamma)^2} \tag{4.29}$$

Where

$$\Gamma = \frac{1}{\tan(\theta_{\mathrm{VH}})}\sqrt{\frac{2}{l_{\mathrm{v}}W}\tanh\left(\frac{W}{2l_{\mathrm{v}}}\right)}$$

Therefore ρ and the standard deviation of the Lorentzian Γ are inversely proportional.
If we do the anti-Fourier transform of this equation to get the position dependent Non-local resistivity we get

$$\mathcal{F}^{-1}\left[\frac{R_{xx}}{1+(k/\Gamma)^2}\right] = \frac{1}{2}\rho W\Gamma e^{-|x|\Gamma} =$$

$$= \frac{\rho W}{\tan(\theta_{\mathrm{VH}})}\sqrt{\frac{2}{l_{\mathrm{v}}W}\tanh\left(\frac{W}{2l_{\mathrm{v}}}\right)}\exp\left[\frac{-|x|}{\tan(\theta_{\mathrm{VH}})}\sqrt{\frac{2}{l_{\mathrm{v}}W}\tanh\left(\frac{W}{2l_{\mathrm{v}}}\right)}\right] \quad (4.30)$$

Since $\tan(\theta_{\mathrm{VH}}) = \rho\sigma_{\mathrm{v}}$, for $\rho \to +\infty$ the equation above converges pointwise to the following saturation constant S

$$\lim_{\rho\to\infty}\mathcal{F}^{-1}\left[\frac{R_{xx}}{1+(k/\Gamma)^2}\right] = \frac{1}{\sigma_{\mathrm{v}}}\sqrt{\frac{2W}{l_{\mathrm{v}}}\tanh\left(\frac{W}{2l_{\mathrm{v}}}\right)} \equiv S \quad (4.31)$$

Second regime and third regime

Now that we have calculated how it behaves in the regime where is similar to a Lorenztian, let's calculate the second regime. We have already calculated the value the plateau assumes in equation 4.4

$$R_{\mathrm{NL}}(k) \approx \rho W\cos^2(\theta_{\mathrm{VH}}) \quad (4.32)$$

While in the third and last regime

$$R_{\mathrm{NL}}(k) \approx \frac{2\rho}{k}\cos^2(\theta_{\mathrm{VH}}) \quad (4.33)$$

Notice how the equations for the second and third regime are both proportional to $\rho\cos^2(\theta_{\mathrm{VH}})$. This means we can write equation 4.27 as approximately

$$\lim_{\rho\to\infty} R_{\mathrm{NL}}(k) = \frac{R_{xx}}{1+(k/\sigma)^2} + \rho\cos^2(\theta_{\mathrm{VH}})C(k) \quad (4.34)$$

Where $C(k)$ is a function that doesn't depend on ρ or $\tan(\theta_{\mathrm{VH}})$ and it comprehends the second, third regime and eventual corrections in between the approximations[1].
Now let $G(x)$ be it's Fourier anti-transform, then we have that

[1]The corrections also are proportional to $\rho\cos^2(\theta_{\mathrm{VH}})$

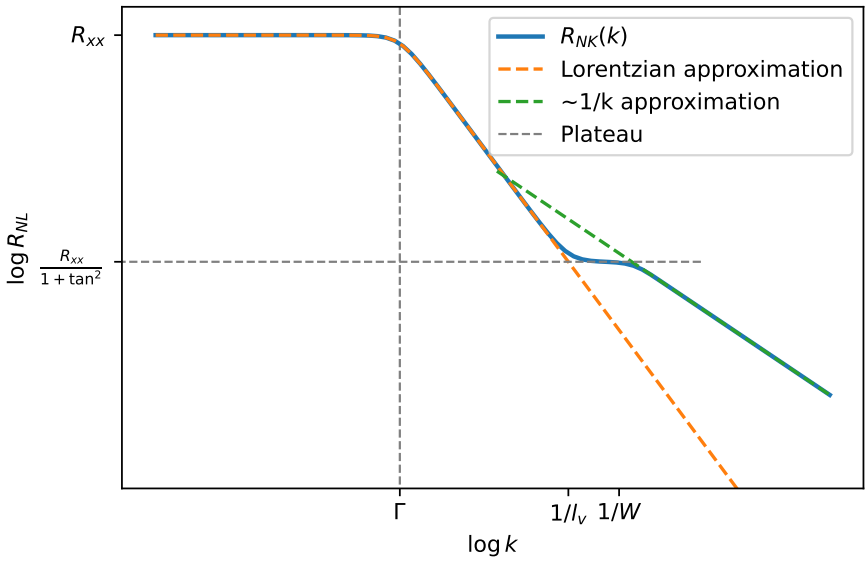

Figure 4.10: The main regimes of this function

$$\lim_{\rho\to\infty} R_{\mathrm{NL}}(x) = S + \frac{1}{\rho}G(x) \tag{4.35}$$

Where here we have used that $\lim_{\rho\to\infty} \rho\cos^2(\theta_{\mathrm{VH}}) = 1/\rho$. This means that for $\rho \to +\infty$ the right hand side term vanishes, unless it diverges. And indeed $G(x)$ diverges for $x = 0$. Therefore, the limit above has pointwise convergence in $\{x \in \mathbb{R} \,|\, x \neq 0\}$

$$\lim_{\rho\to\infty} R_{\mathrm{NL}}(x) = \frac{1}{\sigma_{\mathrm{v}}}\sqrt{\frac{2W}{l_{\mathrm{v}}}\tanh\left(\frac{W}{2l_{\mathrm{v}}}\right)} \qquad \text{for } x \neq 0 \tag{4.36}$$

4.2.3 Putting it all together

The main result from subsection 4.2.1 we showed that for $\tan^2(\theta_{\mathrm{VH}}) \ll 1$ we had equation 4.24

$$R_{\mathrm{NL}}(x) = \frac{2\rho}{\pi}\ln\left|\coth\left(\frac{\pi x}{2W}\right)\right| + \rho^3 F(x) + o(\rho^5)$$

While, in subsection 4.2.2 we had that for $\tan^2(\theta_{\mathrm{VH}}) \gg \sqrt{1+W^2/(4l_{\mathrm{v}}^2)}\tanh\left(\sqrt{1+W^2/(4l_{\mathrm{v}}^2)}\right)$ (eq. 4.26) we had equation 4.36.

$$R_{\mathrm{NL}}(x) = \frac{1}{\sigma_{\mathrm{v}}}\sqrt{\frac{2W}{l_{\mathrm{v}}}\tanh\left(\frac{W}{2l_{\mathrm{v}}}\right)}$$

If we plot the approximations on top of the actual function we get something that looks like figure 4.11

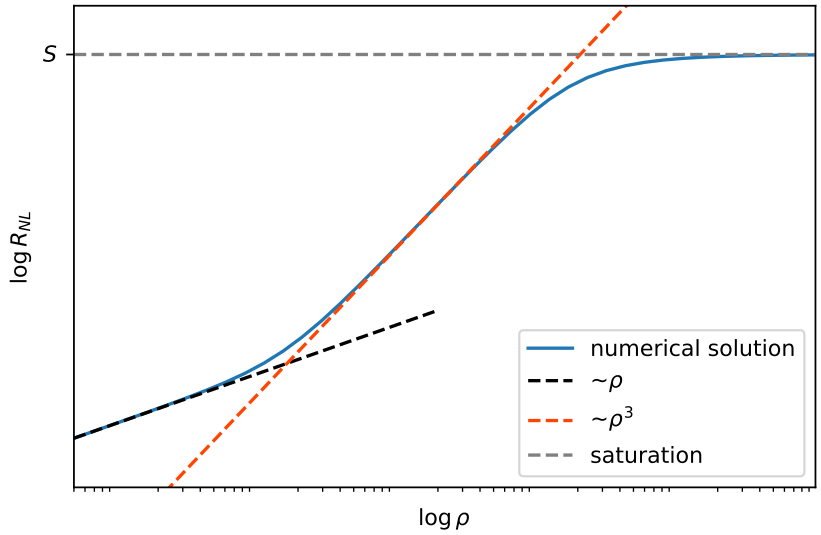

Figure 4.11: The main regimes of this function

4.2.4 Altertative way of studying $R_{\mathbf{NL}}(x)$ as we change ρ

Up until now we have studied $R_{\mathrm{NL}}(x)$ as we change ρ starting directly from the frequency response function (eq. 4.1). This is the most rigorous way for doing this analysis, but it can be cumbersome to work with and doesn't really offer much insight in the topology behind.

A much simpler, but less rigorous way of approaching the problem would be to start from the approximate form of $R_{\mathrm{NL}}(x)$ (eq. 4.19). As you might remeber, this equation had the advantage of being able to distinguish the ohmic effect from the topological ones giving us a strong tool to be able to analyze the graphs.

From image 4.12 it is clear that the linear part at low $\tan(\theta_{\mathrm{VH}})$ is due to the ohmic effect. This makes sense even intuitively, infact the current will prefer choosing the path of least resistance, and since at low $\tan(\theta_{\mathrm{VH}})$ the ohmic resistivity is much less than the hall resistivity, we have a mostly ohmic behavior.

This image also shows that the topological component is the one responsible for the ρ^3 behavior, and then the saturation value.

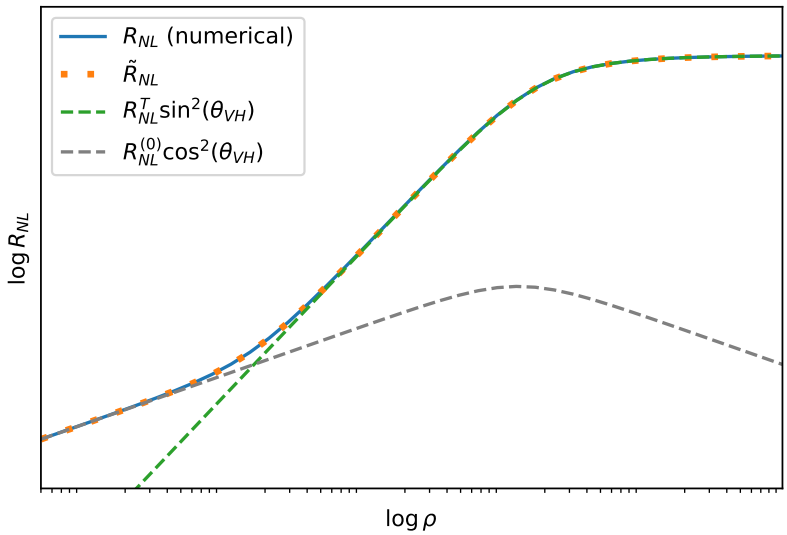

Figure 4.12: R_{NL} (continuous blue line, calculated numerically) and its approximation $\tilde{R}_{\mathrm{NL}}$ (dotted orange line) are virtually indistinguishable. The topological component of $\tilde{R}_{\mathrm{NL}}$ is the green dashed line and the ohmic is the grey dashed line.

A few small details

In the discussion about R_{NL} as we change ρ we choose parameters to highlight the behaviors we talked about. However sometimes certain behaviors disappear, for example if we increase the ohmic contributions by decreasing the width of the bar, figures 4.11 and 4.12 become like in figure 4.13

In the following section we'll see how this applies to lab measurements

4.2.5 Shortcomings of the model

The main shortcoming of the model is that we don't explore the temperature dependence of the system, while we can expect that such effect to be noticeble will need to happen at low temperature CONTINUA

Does this generalize?

Up until now we talked about valley currents, however this also applies to spin-hall effect and spin-orbit effect since the differential equations that govern the system are equivalent

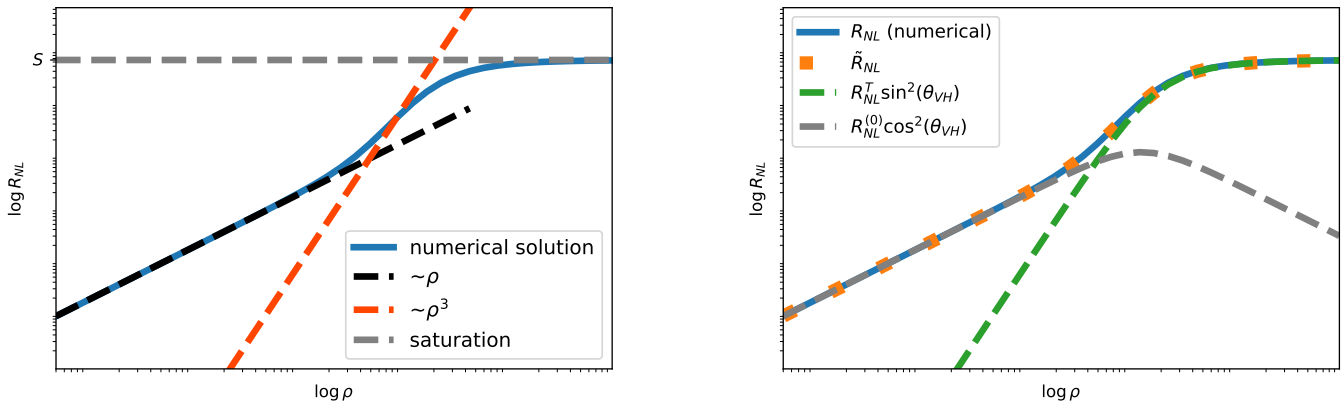

Figure 4.13: As you can see the ρ^3 behavior disappeared

4.3 Comparison with experimental data

Experimental setups have a few limitations compared to the theoretical treatment, for example you don't have complete freedom of changing the resistance, rather the resistance is changed by changing the temperature of the sample. This has a few consequences:

- Since out sample is a semiconductor, the lower the temperature, the higher the resistance, but if the temperature gets too low we enter the ballistic regime, and our treatment is no longer valid.
- If the temperature gets too high, the quantization of the hall effect disappears

This restricts us to a couple order of magnitude of the resistivity.

Now we compare the results with the experimental data. Let's start from analyzing the data from [19].
In this paper the authors measured the valley hall effect of a heterostructure made of bilayer-graphene on top of boron nitride at different angles ϕ between the graphene and the boron nitride. The sample has a width $W = 1.7\mu$m, and inter-valley scattering length $l_{\mathrm{v}} = 1.6\mu$m and the distance of the contact from the injection point is $x = 2.3\mu$m

The angles ϕ that were explored are $0, \pi/6$ and $\pi/3$. If you plot the measurements you get figure 4.14

Now we analyze them one by one

- For $\phi = \pi/3$ we have that the response is fully ohmic, and so we get a completely linear response (figure 4.15)

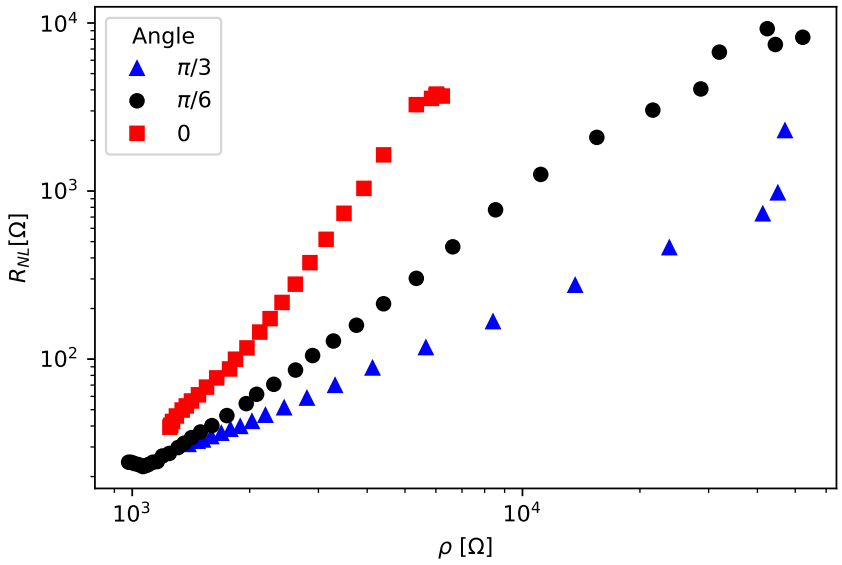

Figure 4.14: Datapoints from [19]

- For $\phi = \pi/6$ we have a hall effect, however, since $W \approx l_v$ the ohmic and the topological response mix together, so we never see the full-fledged ρ^3 behavior.[2]

[2] A more detailed explanation was given in the details of subsection 4.2.4

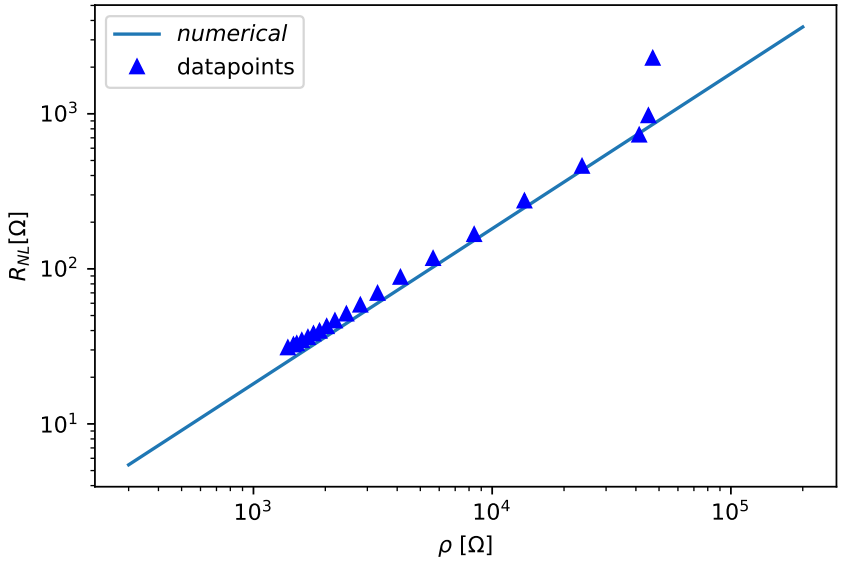

Figure 4.15: Comparison between the data points and the theoretical expectation for $\phi = \pi/3$. The last point is an outlier, but all in all it looks pretty good

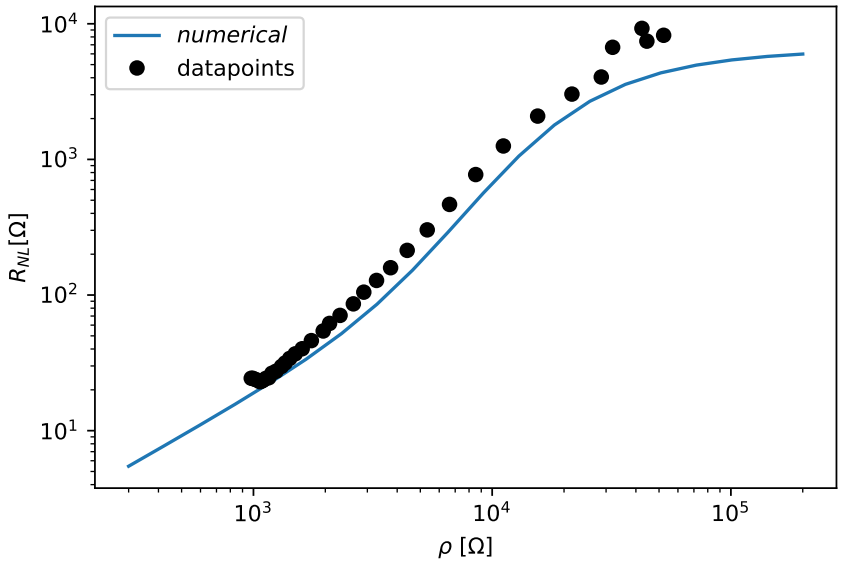

Figure 4.16: Comparison between the data points and the theoretical expectation for $\phi = \pi/6$. The model has a lower precision for higher values of ρ, R_{NL}

Bibliography

[1] K. S. Novoselov *et al.*, "Electric field effect in atomically thin carbon films," *Science*, vol. 306, no. 5696, pp. 666–669, 2004. DOI: 10.1126/science.1102896. eprint: https://www.science.org/doi/pdf/10.1126/science.1102896. [Online]. Available: https://www.science.org/doi/abs/10.1126/science.1102896.

[2] A. H. Castro Neto, F. Guinea, N. M. R. Peres, K. S. Novoselov, and A. K. Geim, "The electronic properties of graphene," *Rev. Mod. Phys.*, vol. 81, pp. 109–162, 1 2009. DOI: 10.1103/RevModPhys.81.109. [Online]. Available: https://link.aps.org/doi/10.1103/RevModPhys.81.109.

[3] F. Bloch, "Über die quantenmechanik der elektronen in kristallgittern," *Zeitschrift für physik*, vol. 52, no. 7, pp. 555–600, 1929.

[4] J. C. Slater and G. F. Koster, "Simplified lcao method for the periodic potential problem," *Physical Review*, vol. 94, no. 6, p. 1498, 1954.

[5] G. Grosso and G. P. Parravicini, *Solid state physics*. Academic press, 2013.

[6] R. Gorbachev *et al.*, "Detecting topological currents in graphene superlattices," *Science*, vol. 346, no. 6208, pp. 448–451, 2014.

[7] M. Sui *et al.*, "Gate-tunable topological valley transport in bilayer graphene," *Nature Physics*, vol. 11, no. 12, pp. 1027–1031, 2015.

[8] Y. Shimazaki, M. Yamamoto, I. V. Borzenets, K. Watanabe, T. Taniguchi, and S. Tarucha, "Generation and detection of pure valley current by electrically induced berry curvature in bilayer graphene," *Nature Physics*, vol. 11, no. 12, pp. 1032–1036, 2015.

[9] D. Xiao, G.-B. Liu, W. Feng, X. Xu, and W. Yao, "Coupled spin and valley physics in monolayers of mos 2 and other group-vi dichalcogenides," *Physical review letters*, vol. 108, no. 19, p. 196 802, 2012.

[10] K. F. Mak, K. L. McGill, J. Park, and P. L. McEuen, "The valley hall effect in mos2 transistors," *Science*, vol. 344, no. 6191, pp. 1489–1492, 2014.

[11] J. Lee, Z. Wang, H. Xie, K. F. Mak, and J. Shan, "Valley magnetoelectricity in single-layer mos2," *Nature materials*, vol. 16, no. 9, pp. 887–891, 2017.

[12] S. O. Valenzuela and M Tinkham, "Direct electronic measurement of the spin hall effect," *Nature*, vol. 442, no. 7099, pp. 176–179, 2006.

[13] D. Abanin, A. Shytov, L. Levitov, and B. Halperin, "Nonlocal charge transport mediated by spin diffusion in the spin hall effect regime," *Physical review B*, vol. 79, no. 3, p. 035 304, 2009.

[14] C Brüne *et al.*, "Evidence for the ballistic intrinsic spin hall effect in hgte nanostructures," *Nature Physics*, vol. 6, no. 6, pp. 448–454, 2010.

[15] D. Abanin *et al.*, "Giant nonlocality near the dirac point in graphene," *Science*, vol. 332, no. 6027, pp. 328–330, 2011.

[16] J. Balakrishnan and K. W. Koon, "G., jaiswal, m., castro neto, ah & özyilmaz, b. colossal enhancement of spin–orbit coupling in weakly hydrogenated graphene," *Nat. Phys*, vol. 9, pp. 284–287, 2013.

[17] Z. Wang, C. Tang, R. Sachs, Y. Barlas, and J. Shi, "Proximity-induced ferromagnetism in graphene revealed by the anomalous hall effect," *Physical review letters*, vol. 114, no. 1, p. 016 603, 2015.

[18] M. Beconcini, F. Taddei, and M. Polini, "Nonlocal topological valley transport at large valley hall angles," *Physical Review B*, vol. 94, no. 12, 2016. DOI: 10.1103/physrevb.94.121408. [Online]. Available: https://doi.org/10.1103%2Fphysrevb.94.121408.

[19] E. Arrighi *et al.*, "Non-identical moiré twins in bilayer graphene," 2022. DOI: 10.48550/ARXIV.2205.01760. [Online]. Available: https://arxiv.org/abs/2205.01760.